MSc Biomedical Engineering

Patient-specific Ti dental implants with antimicrobial properties

Master thesis

Xandra van Megen 4157540

Delft University of Technology

Faculty	:	**Mechanical, Maritime, and Materials Engineering (3ME)**
Department	:	**BioMechanical Engineering**
Specialisation	:	**Biomaterials**
Supervisor	:	**Dr. ir. I. Apachitei, Prof. dr. A.A. Zadpoor**
Date	:	**20-02-2020**

TU Delft Delft University of Technology

Challenge the future

Patient-specific Ti dental implants with antimicrobial properties.

By

Xandra van Megen

in partial fulfilment of the requirements for the degree of

Master of Science

in Biomedical Engineering

at the Delft University of Technology,

to be defended publicly on 20-02-2020

Supervisors:	Dr. Ir. I. Apachitei
	Prof. dr. A.A. Zadpoor
Thesis committee:	Prof. dr. A.A. Zadpoor
	Dr. Ir. I. Apachitei
	Dr. Yaiza Gonzalez Garcia

Biomaterials and Tissue Biomechanics Section

Biomechanical Engineering Department

Faculty of Mechanical, Maritime and Materials Engineering

Delft University of Technology

TU Delft

Abstract

Dental implants are used to replace missing teeth. Although the success rate of dental implants is high, complications such as lack of osseointegration and peri-implantitis can occur. In this study a new type of dental implant is designed that mimics the root shape of the to be extracted tooth. These types of implants can be placed directly after extraction. To create these type of implants, CBCT scan, 3DXpert software, and SLM printing techniques are used.

The aim of this current study is to investigate the application possibilities of antimicrobial surfaces created with the PEO process on these new types of dental implants and compare them with standard screw-type implants. Both implant types were analysed in terms of surface morphology, chemical composition, phase composition, Ag ion release profile and in vitro antimicrobial activity.

All surfaces of the implants were successfully treated using the PEO process. The titanium oxide layer was formed homogeneously on all implants and resulted in a microporous surface layer. Using the zone of inhibition test, it was identified that all implants showed antibacterial activity against methicillin-resistant Staphylococcus aureus (MRSA), however a larger growth inhibition zone was identified for porous patient-specific implants than screw-type implants. The ion release test indicated that a higher ion release was found on the porous patient-specific implants with a higher surface area than the screw-type dental implants, which is probably related to the surface area of the implants. This study indicates it is possible to create patient-specific dental implants that show antimicrobial properties against MRSA.

Table of content

1. Introduction

Dental implants are used for over 30 years to replace missing tooth with a success rate of 90% [1, 2]. Although this success rate is high, complications can occur that lead to failure of the implants. Patients with dental implants can develop peri-implant diseases, such as peri-implantitis [1, 2].

Peri-implantitis is a progressive irreversible inflammation of the soft tissue and hard tissue around the implant. If not treated, it can lead to loss of support and failure of osseointegration and eventually to failure [3–5]. Peri-implantitis is found in 6-17% on implants after 10 years [6–8].

Peri-implantitis occurs when primary colonizing bacteria (Streptococcus gordonii, Streptococcus mutans, Streptococcus mitis, Streptococcus oralis and Streptococcus sanguinis) adhere to the implant surface and proliferate. Bacteria will form a biofilm and generate an extracellular matrix (Figure 1). This biofilm is a good environment for late colonizers (Lactobacillus salivarius, Porphyromonas gingivalis, Fusobacterium nucleatum, Aggregatibacter actinomycetemcomitans) [9–15]. When this biofilm is formed, it cannot be eliminated. Therefore, the standard treatment procedure is implant removal. Peri-implantitis creates thus a clinical problem without an optimal treatment [16].

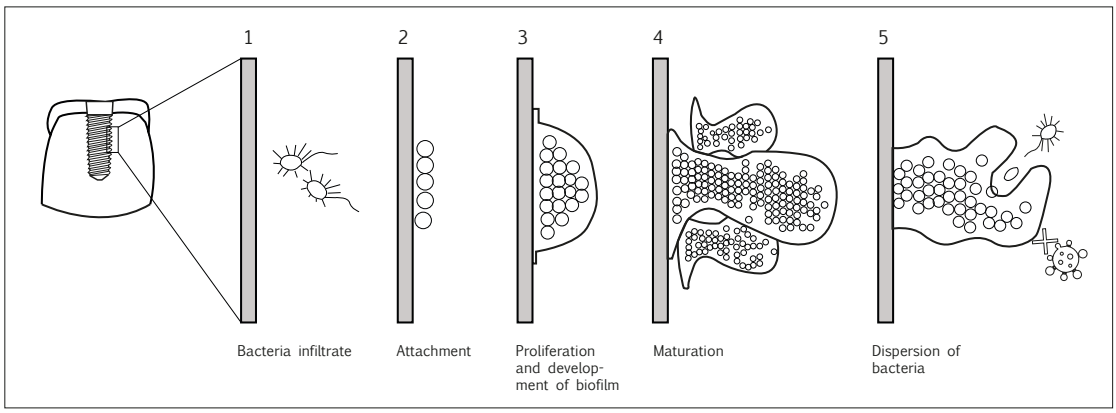

Figure 1: Biofilm formation steps.

Traditionally antibiotics are used to prevent or treat peri-implantitis, but antibiotics are not able to eliminate biofilms. Therefore it is important to prevent bacteria adhesion on the implant surface [17–19]. Promising strategies are surface modification techniques to incorporate inorganic nanoparticles, such as silver [20, 21]. Silver is known to be effective in inhibiting bacterial growth by releasing ions and thereby disrupting bacterial membranes of both Gram-negative and Gram-positive bacteria [22]. Next to that it also generates reactive oxygen species (ROS) [23, 24]. Surface modification techniques are used to incorporate silver nanoparticles on the implant surface for its antimicrobial effect.

Other developments in dentistry are focused on simplifying the implant placement procedure, such as immediate implant placement [25, 26]. In this method implants are inserted directly after extraction. The advantages of this method are reduced treatment time, less surgeries, preservation of the extraction socket, less trauma, improved patient comfort and eventually reduced costs [25–27].

With the current screw-type implant there is one major problem with immediate placement, that is the incongruity between extraction socket and implant shape [25, 26]. The solution to this problem is to use so called root-analogue-implants. These are implants mimicking the root of the extracted tooth. This way the implants are adapted to the shape of the socket instead of adapting the bone socket to the shape of the implant (Figure 2). With this principle patient-specific implants are

created. Due to the developments in scanning techniques, such as cone-beam computed tomography (CBCT), and computer aided design techniques (CAD) and fabrication techniques such as selective laser melting (SLM) printing it is possible to create accurate shaped implants of titanium and its alloys. [28–32]. The advantages of this type of implants are the elimination of bone drills during surgery, and congruency between implant and socket [27, 33–36].

The CAD and SLM techniques are not only limited to creating patient-specific implants, they can also be used to create porous implants to improve its osseointegration properties [32, [37–39]. Implants with a porous structure, created with SLM, have the ability to induce bone in growth [40, 41]. For this an optimal pore size larger than 300 µm is required [42]. Another advantage of porous structure is that the implants stiffness is reduced. Compared to solid implants, porous implants mimic more closely the mechanical properties and structure of bone [43–45].

Although porous structures are beneficial for osseointegration, it also creates a larger surface area onto which bacteria can adhere, leading to peri-implantitis. It is therefore even more important to create an antimicrobial surface on these types of porous implants.

Several surface modification techniques are used to create antimicrobial surfaces on titanium biomaterials, such as spark anodization, plasma electrolytic oxidation (PEO), sol–gel, electrophoresis, electrohydrodynamic atomization, plasma immersion ion implantation, [15], [46]–[49] Among these, the plasma electrolytic oxidation process has certain advantages, such as surface coverage of complex geometries and preservation of mechanical properties [50]. PEO provides a micro/nano porous titanium dioxide layer on the surface in which nanoparticles can be incorporated [50].

The aim of this current study is to investigate the application of antimicrobial surfaces created with the PEO process on dental implants. In this study two types of dental implants are used. Standard screw-type implants and patients-specific implant with a porous structure that were designed in this study. Both implant types are analysed with regard to surface morphology, chemical composition, phase composition, silver ion release and in vitro antimicrobial activity.

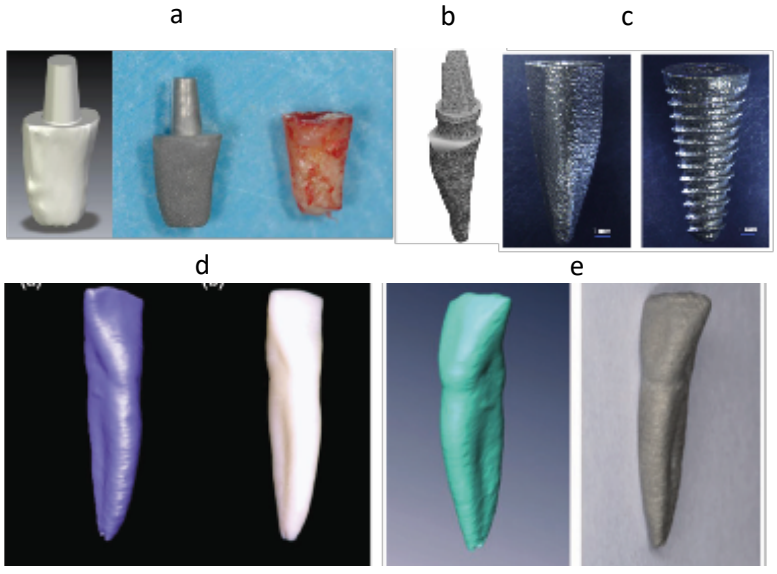

Figure 2: Examples of root-analogue-implants. (a) Root analogue implant [51] (b) Root analogue implant [29] (c) Root analogue implant with screw thread [52] (d) Root analogue implant of zirconium [53] (e) Root analogue implant [54].

2. Materials and methods

In this study two types of dental implants are used. The first type of implants are standard (commercially available) screw-type implants supplied by Dyna Dental Engineering BV (Bergen op Zoom, the Netherlands) and the second type are the newly designed patient-specific implants.

2.1 Overview

In Table 1 an overview of the samples used in this study is shown. In Figure 3 a selection of the four most relevant samples is shown. In Table 2 an overview of the methods for design, manufacturing and physical characterisation is shown.

Table 1: Overview of the samples used in this study.

Abbreviation	Description	Biomaterial	Manufacturing process
Screw-type implants	Dyna Helix ST Octa implants with a d= 3.6 mm and l= 10mm *	Ti6Al4V	Subtractive manufacturing
S300 P780	Implant with s= 300 µm and p=780 µm		Additive manufacturing
S300 P980	Implant with s= 300 µm and p=980 µm		
S400 P650	Implant with s= 400 µm and p=650 µm		
S400 P850	Implant with s= 400 µm and p=850 µm		
S300 P600	Implant with s= 300 µm and p=600 µm		
S400 P500	Implant with s= 400 µm and p=500 µm		
S250 P450	Implant with s= 250 µm and p=450 µm		

**** Supplier Dyna Dental Engineering BV***

***** Dimensions: d=diameter, l=length, s=strut thickness, p=pore size***

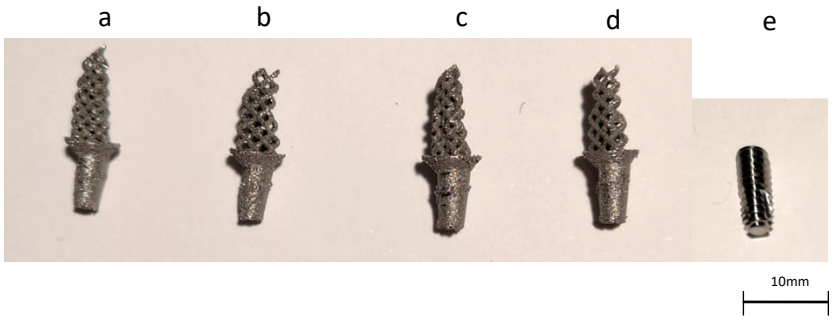

Figure 3: Overview of the implants used in this study. (a) S300 P780 (b) S300 P980 (c) S400 P650 (d) S400 P850 (e) screw-type.

Table 2: Overview of the methods used in this study.

Stage of study	Steps	Methods
Design of novel dental implants	Design	Cone Beam Computed Tomography (CBCT) scan, segmentation software (3D slicer), CAD software (Rhinoceros and grasshopper) Fused Deposition Modelling printer (Ultimaker 2+)
	Manufacturing	Selective laser melting (SLM)
Synthesis of antimicrobial surface	Application of antimicrobial surface with silver nanoparticles	Plasma electrolytic oxidation (PEO)
Characterisation of implants	Surface characterisation and morphology	Scanning electron microscopy (SEM)
	Chemical composition	SEM and energy dispersive spectroscopy (EDS)
	Phase composition of the layer	X-ray diffraction (XRD)
	Ion-release test	Inductively coupled plasma-optical emission spectrometry (ICP-OES)
Antibacterial testing	Bacterial testing against methicillin-resistant Staphylococcus aureus (MRSA)	Zone of inhibition (ZOI)

2.2 Patient-specific implants

The patient-specific implants in this study were designed from scratch. The implants were designed based on a CBCT scan of a real patient and it is assumed that the left lateral incisor needs to be replaced.

2.2.1 Design and manufacturing of a patient-specific implants

For the patient-specific implants the root shape of the extracted root is mimicked and translated into the shape of the implant. The design part of the porous patient-specific implant is divided into 4 steps: (i) Scan of the root; (ii) Image segmentation; (iii) Design of the implant; (iv) Manufacturing.

Before those steps were conducted the specifications for the design were formulated.

2.2.1.1 Specifications

To make the design for the patient-specific implants, certain requirements and specifications were set. First of all, the patient-specific implants need to mimic the exact shape of the original root that needs

to be extracted. This was achieved by making an accurate CBCT scan and transferring this data to a digital 3D model.

To create a porous structure different unit type cells can be used. In this project the diamond unit cell type was chosen. It is a relatively easy shape to print because of its self-supporting structure due to the 45° angles.

The implant needs to function in the human body, therefore the biocompatible material Ti6Al4V was used.

The strut size of the porous structure was limited to a minimum of 300 µm by the resolution of the titanium SLM machine (SLM-125, Realizer GmbH, Borchen, Germany).

The implant should facilitate an abutment. In this design the abutment is fixed on the implant, which leads to a one-piece implant design. In screw-type implants the abutment is a separate part, because the position can be slightly changed if needed. In the case of patient-specific implants the slight changeability is not required, because the fit of the implant into the extraction socket also secures the exact right position and direction. Less moving and separate parts also reduces the risk of failure and infection. In this study the replaced tooth is a lateral incisor which is in the aesthetic zone. Cemented crowns are therefore preferred and the design will be adjusted on this type of crown attachment.

The porous part of the implant was surface treated using the PEO process to create an antimicrobial surface. For the PEO process it was necessary to attach the implant to the anode connector. An innovative solution to use the abutment as connector was created. This way the abutment was connected with the entire porous part of the implant to let the current flow through.

2.2.1.2 Scanning of the root to obtain a 3D model

In order to obtain the exact dimensions of the original root, a CBCT scan was made while the tooth was still in the patient's jaw. For this study a CBCT scan from incisix was used. The upper left lateral incisor is the to-be-replaced-tooth in this study, because this tooth is in the aesthetic zone of the mouth. A main reason to develop patient-specific implants is to reduce treatment time, which is especially relevant for teeth in the aesthetic zone.

2.2.1.3 Image segmentation

Using segmentation software, 3D slicer (Version 4, Slicer, Boston, United Stated of America), the root of one particular tooth was isolated. In this case the upper left lateral incisor. First the threshold for bone was set, which shows only the bone parts of the scan. By using the selection tool, the tooth and

root were selected of which a 3D model was created. This is saved as an STL file (Figure 4).

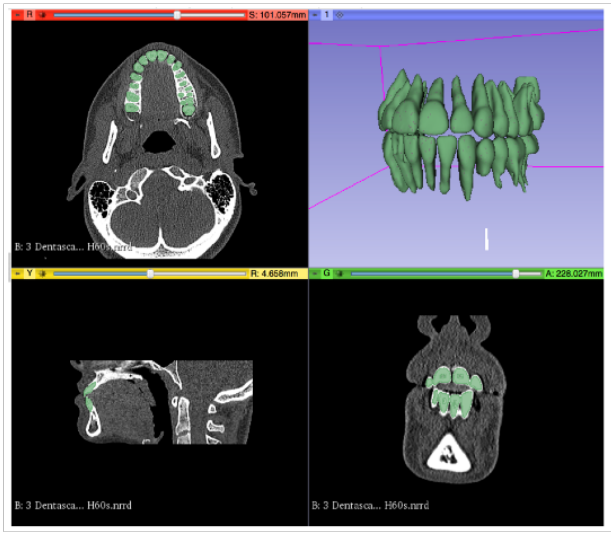

Figure 4: 3D slicer image segmentation.

2.2.1.4 Design of the implant

After obtaining the STL model from the CBCT scan and image segmentation the crown part needs to be disconnected from the root part. This was done in Rhinoceros software. The abutment was designed in Rhino3D (Rhinoceros, Robert McNeel & Associates, USA) as well. A normal type of abutment which has a flat part on the buccal side was designed.

The porous structure was created using 3DXpert software (3DSystems, USA). The parameters were set on diamond unit whole cell, an variable parameters were used for strut thickness of 250 µm, 300 µm and 400 µm and a changing cell size varying from 0.7, 1.0, 1.2 and 1.4.

The differences in dimensions compared to the original root shape were analysed in Geomagic studio 12 software (3DSystems, USA).

2.2.1.5 Manufacturing with FDM and testing

Before printing the implants from Ti6Al4V, the models were printed with a fused deposition modelling (FDM) printer, Ultimaker 2+ (Ultimaker BV, Utrecht, The Netherlands). The models were scaled up 3 times, because the accuracy of the FDM printer was not high. The main purpose of this printing was to test the fitting of the implants in the socket and to prove the concept.

2.2.2 Manufacturing with selective laser melting

Manufacturing of the dental implants was done using SLM (Realizer GmbH, Borchen, Germany). The design of the implant was saved into an STL file and this was imported in the printer software. Medical grade Ti6Al4V spherical particles powder were used. A layer-by-layer printing approach was used. The design was sliced into layers of 50 µm. The accuracy of the printer limits the strut thickness to a minimum of 300 µm.

The abutment of the implant was supported with support material. In this case these were weaker struts, which was required for printing. These struts were also the connection between the printed object and the building platform. After printing, the loose powder was removed by a vacuum cleaner.

Afterwards the support material was removed. Lastly, the implants were ultrasonically cleaned in acetone, ethanol and demineralised water (5 minutes in every liquid solution).

2.3 Synthesis of antimicrobial surfaces

2.3.1 Plasma electrolytic oxidation

An antimicrobial surface on the dental implants is created to prevent infection after implantation. To create an antimicrobial surface on the dental implants, PEO process was used.

2.3.1.1 Equipment

For the PEO process the following devices are required: electrolytic cell, anode (the implant), cathode (stainless steel cylindrical part), stirrer and beakers, AC power supply (50Hz, ACS 1500, ET Power Systems Ltd., United Kingdom, thermostatic bath and pump (Thermo Haake V15, Karlsruhe, Germany), a PC linked with the AC power supply though a data acquisition board NI SCXI-1000 (Austin, Texas, United States).

2.3.1.2 Experimental conditions

Two electrolytes were prepared in this study. One electrolyte consisted of 3.36 g calcium glycerophosphate (Ca-GP) (Dr. Paul Lohmann GmbH, Emmerthal, Germany), 19,2 g calcium acetate (CA) (Sigma-Aldrich, St. Louis, USA) and 800 ml demineralised water. The other electrolyte consisted of similar solution content but additionally included 2.4 g silver nanoparticles (Sigma-Aldrich, St. Louis, USA). Both electrolytes were stirred at 500 rpm and cooled till a temperature between 4-6 °C was reached.

The dental implants samples were placed in the electrolyte. Since all samples have a different porosity the surface areas differ. A current density of 20A/dm^2 for 300 s was applied for the oxidation process. The surface areas and current densities for all samples are given in Table 3.

Table 3: Surface area and current density of dental implant samples.

	S300 P780	**S300 P980**	**S400 P650**	**S400 P850**	**Screw-type**
Surface area (mm^2)	185.6	134.8	206.0	161.9	133.5
Applied current (mA)	371	270	412	324	267

The voltage-time transients were recorded in intervals of 1 s through a National Instruments SCXI data acquisition system.

After 300 s the dental implants were taken out of the electrolyte and cleaned in running tap water for one minute. Thereafter, the implants were dried by a compressed air device.

2.4 Characterisation of the implants

2.4.1 Surface characterisation and morphology

The characterisation of the surface and the morphology of the surface of the dental implants was analysed using a scanning electron microscopy (SEM) JSM-IT100 (JEOL, Tokyo, Japan). To acquire images, the following settings were used: SED, voltage of 5 - 20keV, working distance of 10-12mm. For implants treated with silver nanoparticles the backscattered electron mode was selected.

2.4.2 Chemical composition

The chemical composition of the implants was analysed with energy dispersive spectroscopy (EDS). The SEM was equipped with the EDS detector to measure the chemical composition on different spots of the implant. The elements to measure were: Al, Ti, V, P, O, Ca and Ag.

2.4.3 Phase composition of the layer

The phase composition of the layer of the implants after PEO without silver particles was analysed by X-ray diffraction (XRD). The settings for the screw-type implants differed from the settings of the patient-specific implants due to the complexity of the structure.

The following settings were applied for the screw-type implants:
The analysis was performed on a Bruker D8 (Bruker Billerica, Massachusetts, USA) Advance diffractometer Bragg-Brentano geometry with graphite monochomator and Vantec position sensitive detector. Co-Kα radiation, 45 kV 35 mA. Specimen holder SA52. Scatter screen height 5mm. Measurements were performed with coupled θ -2θ scan 20° - 120°, step size 0.034 ° 2θ, counting time per step 2 s. Evaluation of the data was done with Bruker software DiffracSuite.Eva version 5.0.

The following settings were applied for the patient-specific implants:
The analysis was performed on a Bruker D8 (Bruker Billerica, Massachusetts, USA) Discover with Eulerian cradle with parallel beam geometry. Co-K_α radiation, 45 kV 25 mA. Specimen holder HP42. Scatter tube. Measurements were performed with coupled θ-2θ with a scan range 20° - 135°, step size 0.04 ° 2θ, counting time per step 0.2 s. Evaluation of the data was done with Bruker software DiffracSuite.Eva version 5.0.

2.4.4 Ion-release test

To investigate the release characteristics of silver ions release over time an ion-release test was performed. Samples with silver nanoparticles were immersed in 1 ml phosphate buffered saline (PBS) (VWR Life Science, USA) in dark Eppendorf vials. The Eppendorf vials were place in a water bath with a constant temperature of 37°C. After 0.5 day, 1 day, 2 days, 4 days, 7 days, 14 days and 28 days the PBS was collected and refreshed. The collected PBS at every time point was analysed with inductively coupled plasma-optical emission spectrometry (ICP-OES, Thermo Fisher Scientific, Waltham, Massachusetts, USA). Using this method, the concentration of silver ions released was quantified.

2.5 Zone of inhibition

For antibacterial testing the implants with silver nanoparticles (S300 P780 & S300 P980 & S400 P850 and screw-type implants) were exposed to methicillin-resistant *Staphylococcus aureus* (MRSA USA300). The inhibitory leaching activity of the silver nanoparticles on the surface of the implants could be observed using the zone of inhibition method. First the implants were sterilized by heat treatment using an oven. The implants were in the oven (UT6, Thermo Scientific Heraeus) for one hour at 110°C.

A fresh bacterial inoculum was prepared by a suspension of a MRSA USA300 colony to 3ml fresh tryptic soy broth (TSB) medium in a 15ml tube. This tube was incubated on a shaking platform for 3 hours at 37°C. After 3 hours the tubes were vortexed. The optical density was measured at a wavelength of 600nm with a spectrometer (GENESYS 20 Thermo Spectronic, Thermo Fisher Scientific, USA) and incubated till an optical density of 600n :0.5, to make sure that the bacteria are in the log phase.

Thereafter the fresh cultures were dilutes in TSB broth to an optical density of 600 nm: 0.01 ($1*10^7$ CFU/ml).

The preparation of the Luria-Bertani-agar plates was done by boiling the agar using a microwave and pouring it into sterile petri dishes. After cooling down and solidifying of the LB agar, a sterile swab is used to evenly spread the bacteria on the agar plates (optical density of 600nm: 0.01 with (1*10^7 CFU/ml bacteria). Each time the plate is turned 90° until the plate was fully covered with bacteria. After spreading the bacteria, the implants (3 of each sample) were pressed into the agar on the plate. The plates are incubated overnight at a temperature of 37°C. During the incubation bacteria will grow and a zone of inhibition around the implants was observed due to the leaching activity of the of the silver nanoparticles. A photo of the plates was taken with Image Quant LA24000 (GE healthcare). To quantify the zone of inhibition ImageJ software was used.

Before the start of this test, the edge of abutment of the implants was removed by filing in order to press the porous part of the implants in the agar layer.

3. Results

The first sections of the results (3.1 and 3.2), are only focused on the patient-specific implants since these sections consider the design and manufacturing of the implants. The screw-type implants were not designed or manufactured in this study, but provided by Dyna Dental Engineering BV. In the sections about the antimicrobial surfaces (3.3-3.8) a division is made between the screw-type implants and the patient-specific implants.

3.1 Dimensions and deviations of the patient-specific implant compared to the original shape

In Figure 5, a picture of several different porosity model is shown in which the deviation between the porous implant was compared with the original root shape. In Table 4 the RMS error is given. This value indicates the deviation error between the original shape and the porous structure.

As can be seen in Figure 5 and Table 4 the implants with a lower unit cell size (smaller pores) had a lower RMS error than the samples with a higher unit cell size. This means that the shape with a low porosity fitted better with the original shape. It can be said that if the unit cell size increases, the RMS error becomes larger, which means a lower accuracy.

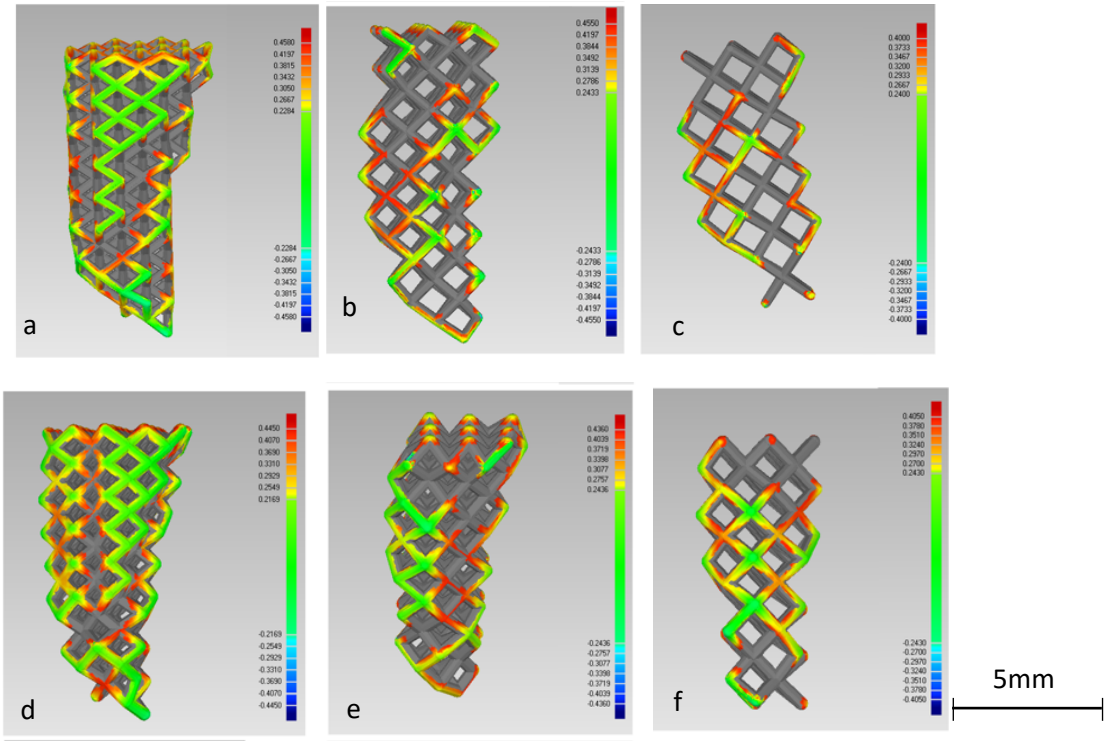

Figure 5: Deviation of the porous samples compared with the original shape. (a) S300 P600 (b) S300 P780 (c) S300 P980 (d) S400 P500 (e) S400 P650 (f) S400 P850.

Table 4: Alignment deviation of the porous samples to the original shape. The samples are aligned to the original root shape. In the table RMS error is given.

Sample	S300 P600	S300 P780	S300 P980	S400 P500	S400 S650	S400 S850
RMS error	0.28	0.40	0.52	0.27	0.40	0.48

3.2 Fabrication of the patient-specific implants

3.2.1 FDM printed implants

The first implants were printed with an FDM printer Ultimaker 2+ (Figure 6). This was done to test the concept of patient-specific dental implants that are placed in the extraction socket. To test this the implants were scaled 1:3. In figure 6 the scaled implants are shown. A scaling of 0.1 in either x or y direction was needed to let the implant fit in the extraction socket. This proved the main principle of this patient-specific-dental-implant-concept: a dental root can be scanned, printed and inserted into the exact same socket. However, this FDM method of printing was different and less accurate than the SLM printer that will be used for the titanium dental implants.

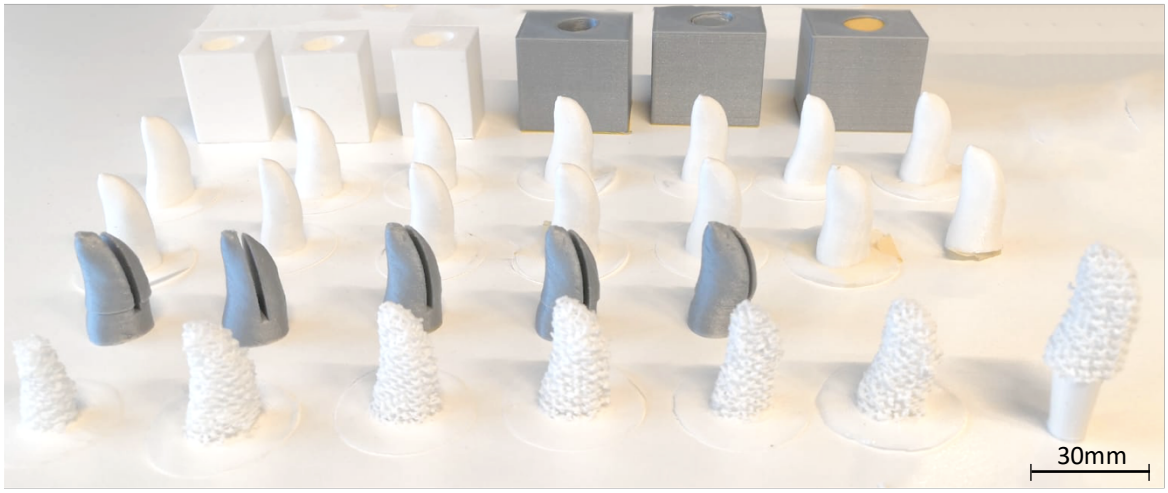

Figure 6: FDM printed implants, scaled 3 times to test fitting and proof concept.

3.2.2 SLM printed implants

In Figure 7 an SLM Ti6Al4V printed implant is shown. It shows the implant with support material on the building plate, implant with support material, and the implant after support removal.

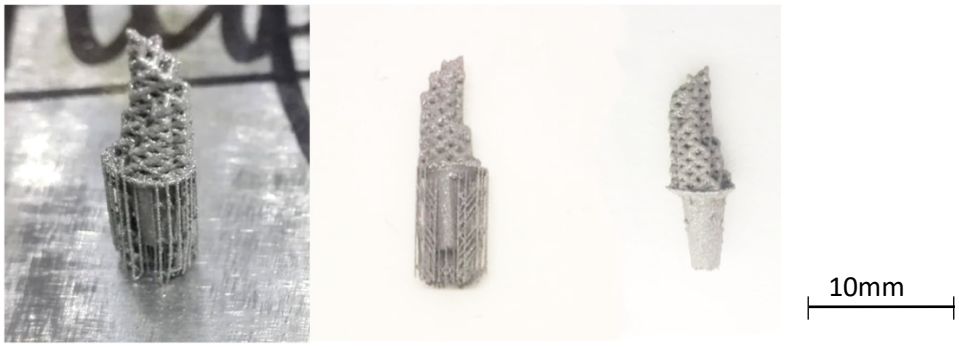

(a) (b) (c)

Figure 7: Additive manufactured implants with SLM. (a) Implant with support material on building plate. (b) Implant with support material. (c) Implant after support removal.

3.2.3 SLM printed implants compared to STL models

In Figure 8 an overview of the samples used in this study is shown, including the STL model with the dimensions of the pores and the struts and including SEM images of the printed implants with dimensions of the pores and struts. After observing the samples with SEM it was found that the pores of the samples differ from the dimensions of the STL models. In all samples the strut size was larger,

resulting in a smaller pore size. Some pores are larger than others and a considerable amount of the them were not complete pores. This is especially the case in the S250 P450 sample. In Table 5, the average sizes of the strut size and pore size were given for all samples.

By increasing the unit cell size, a homogenously and evenly distributed pores were obtained. This was visible in the samples S300 P780, S300 P980, S400 P650, and S400 P850. These four samples are used in this study.

Table 5: Strut thickness and pore size of the STL model VS SLM printed model.

Sample	**Strut thickness (S) and pore size (P) in µm**	
	STL model	**3D Printed**
S250 P450	S= 250	S= 250-350
	P= 450	P= 200-400
S300 P600	S= 300	S= 300-450
	P= 600	P= 300-600
S400 P500	S= 400	S= 400-500
	P= 500	P= 350-500
S300 P780	S= 300	S= 400-480
	P= 780	P= 550-800
S300 P980	S= 300	S= 400-480
	P= 980	P= 750-1000
S400 P650	S= 400	S= 400-550
	P= 650	P= 530-630
S400 P850	S= 400	S= 460-550
	P= 850	P= 600-900

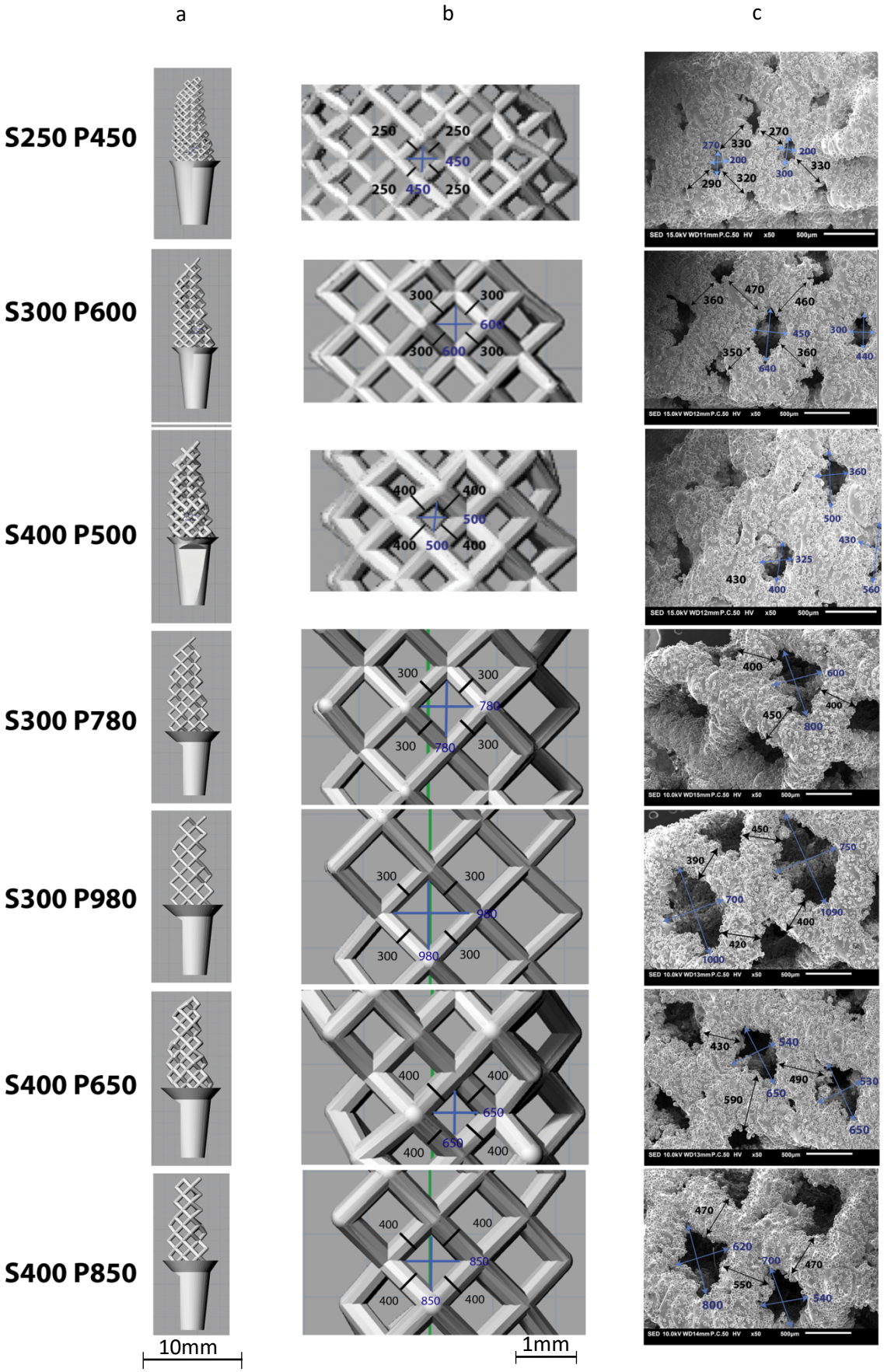

Figure 8: Verification of additive manufactured implants. (a) STL models (b) Magnified from STL model (c) SEM images of the additive manufactured implants. Numbers are dimensions given in µm.

3.3 Voltage-time response of the PEO process

The PEO process was used to create the antimicrobial surface. The PEO biofunctionalization on the screw-type implants and patient-specific implants was successful. During the PEO process the voltage-time (V-t) response was recorded. The graph shows the typical behaviour. In the first steep part of the graph, the titanium oxide layer was thickened. Thereafter the dielectric breakdown occurred in which the calcium and phosphor (as well silver) incorporate onto the surface.

In Figures 9 and 10, the V-t responses of PEO-treated and PEO + Ag treated implants on respectively screw-type implants and patient-specific implants are shown.

For the screw-type implants a final voltage of 240V after 300 seconds was measured (Figure 9 and Table 6), which was higher than the final voltage of 190V for the patient-specific implants (Figure 10 and Table 7). For both implant types the voltage for the PEO + Ag treated samples was lower compared to the only PEO-treated samples. The V-t diagram of the S400 P650 PEO + Ag sample showed a different behaviour. After 220 seconds the voltage dropped till a level of 50V and continued from there.

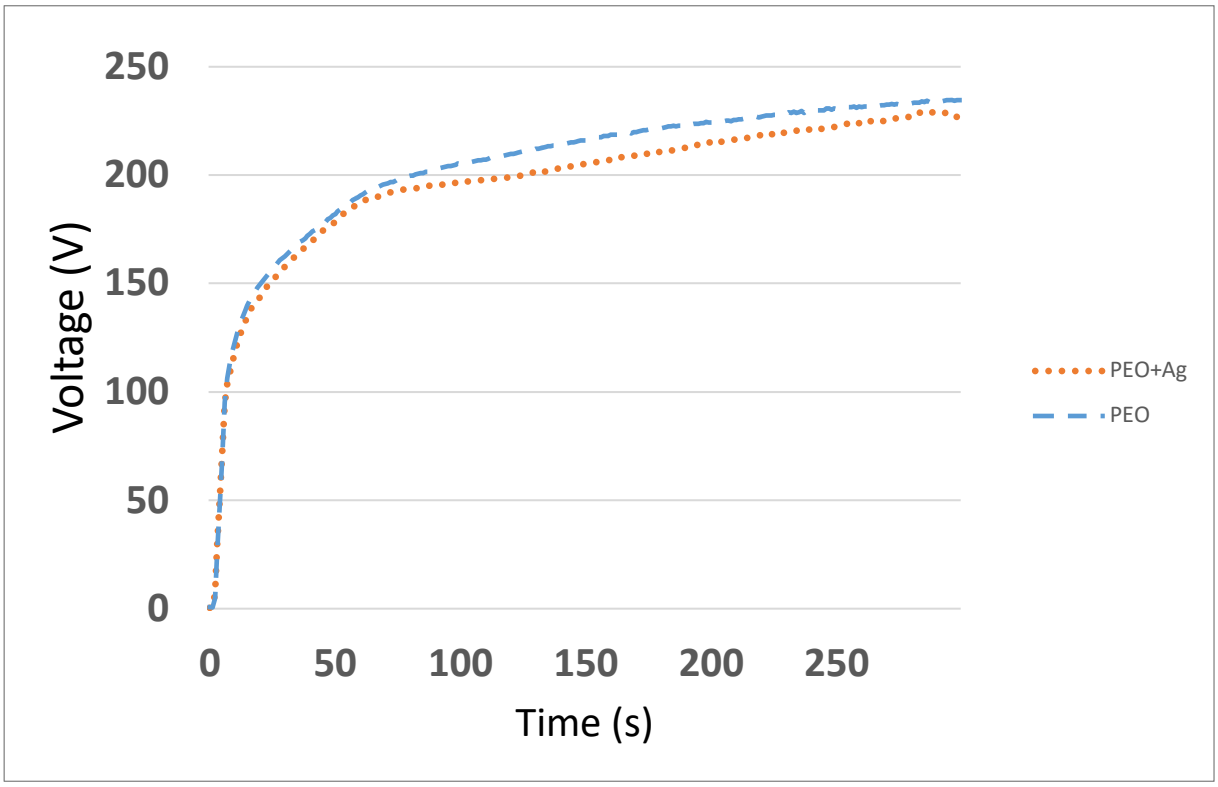

Figure 9: Voltage-time response of PEO and PEO + Ag-treated screw-type implants.

Table 6: Voltage-increase rate of PEO an PEO + Ag-treated screw-type implants.

Sample	$(dV/dt)_1/(V\ s^{-1})$	$(dV/dt)_2/(V\ s^{-1})$	V_{sp}/V	V_f/V
PEO	4.8	0.89	167	235
PEO+Ag	4.7	0.87	165	230

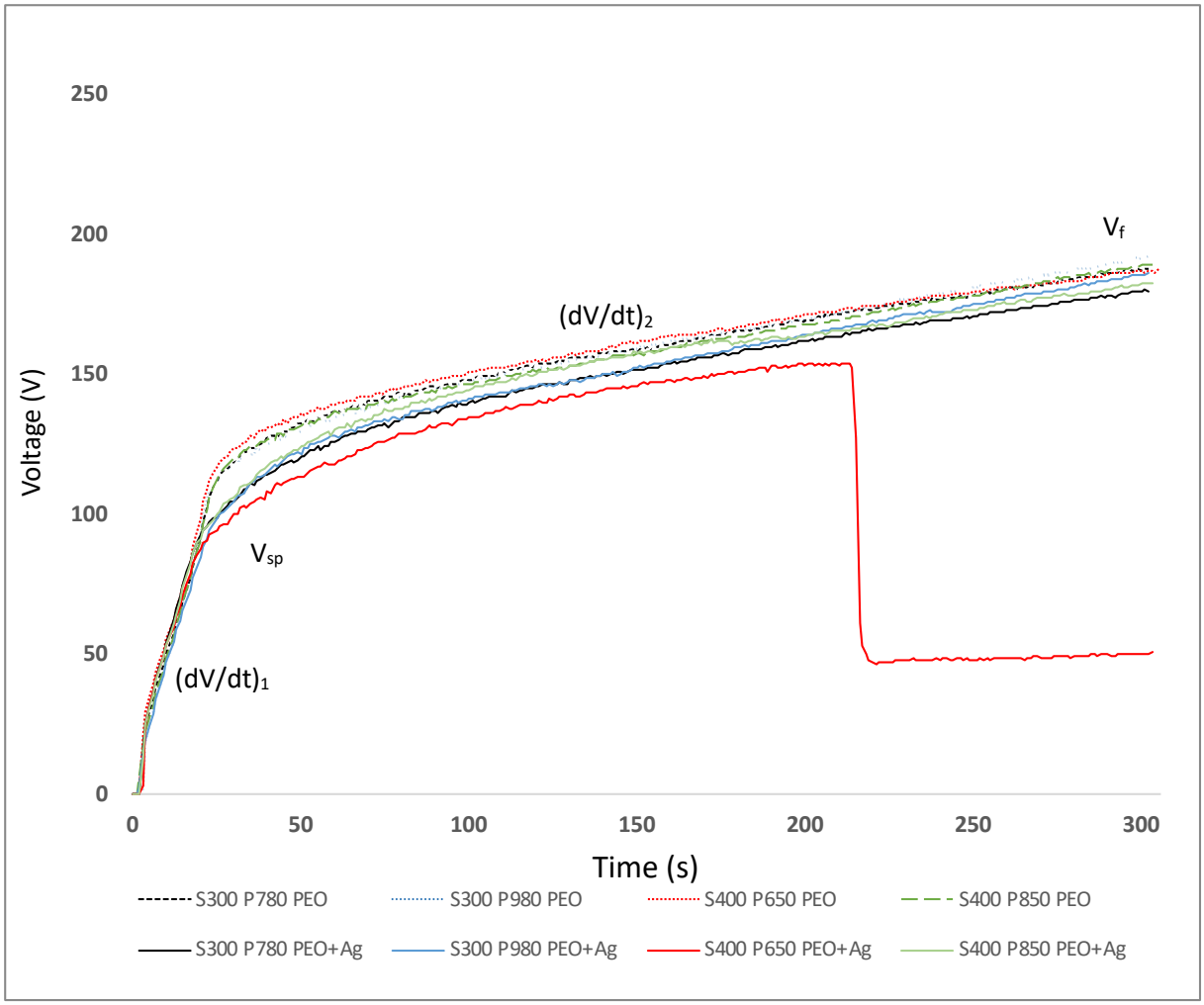

Figure 10: Voltage-time response of PEO and PEO + Ag-treated patient-specific porous implants.

Table 7: Voltage increase rate of PEO and PEO + Ag-treated patient-specific porous implants

Sample	$(dV/dt)_1/(V\ s^{-1})$	$(dV/dt)_2/(V\ s^{-1})$	V_{sp}/V	V_f/V
S300 P780 PEO	4.1	0.69	119	188
S300 P780 PEO+Ag	2.9	0.69	112	180
S300 P980 PEO	3.9	0.71	118	191
S300 P980 PEO+Ag	2.9	0.71	112	186
S400 P650 PEO	4.3	0.68	121	186
S400 P650 PEO+Ag	2.5	-	119	-
S400 P850 PEO	4.1	0.70	119	189
S400 P850 PEO+Ag	3.0	0.69	116	182

3.4 Surface characterisation and morphology

The SLM patient-specific implants changed colour after PEO treatment; the colour became dark grey. After PEO with silver (Ag) nanoparticles they turn into an even darker colour (Figure 11).

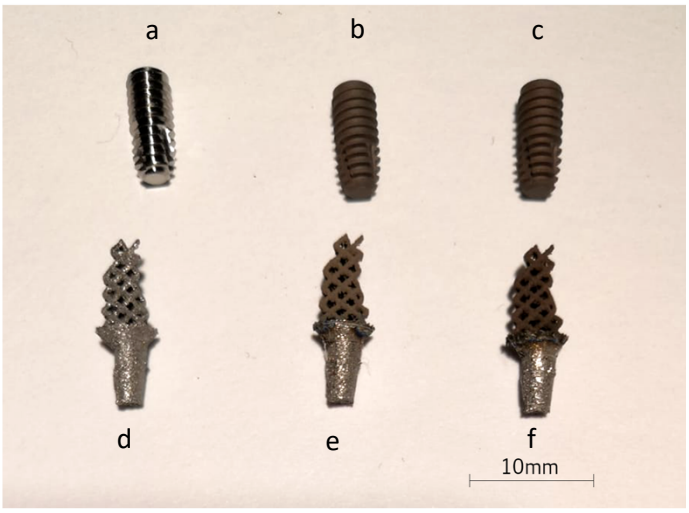

Figure 11: Screw-type implants and patient-specific implants. (a) Non-treated implant (b) PEO-treated implant (c) PEO +Ag treated implant (d) Non-treated implant (e) PEO-treated implant (f) PEO +Ag treated implant.

A titanium oxide layer was formed homogenous over the surface according to the SEM images, consisting of homogenous spread micro- and nanoporosity. The nanoporous structure was clearly visible on the SEM images for the PEO-treated and PEO + Ag treated samples (Figures 12 and 13, Appendix I). This was the case for all different samples with different porosities, including the screw-type sample. No clear difference was found between PEO and PEO + Ag treated samples.

On the screw-type implants the sharp edges of the screw-threads became smoother after PEO treatment. The growing oxide layer does not follow the sharp edge that was created after machining (Figure 12, Appendix I). On the patient-specific implants no clear difference could be observed on the geometry. No sharp edges were created due to the small powder particles used for printing.

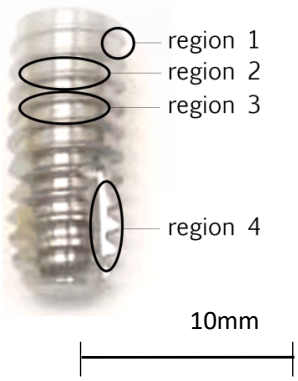

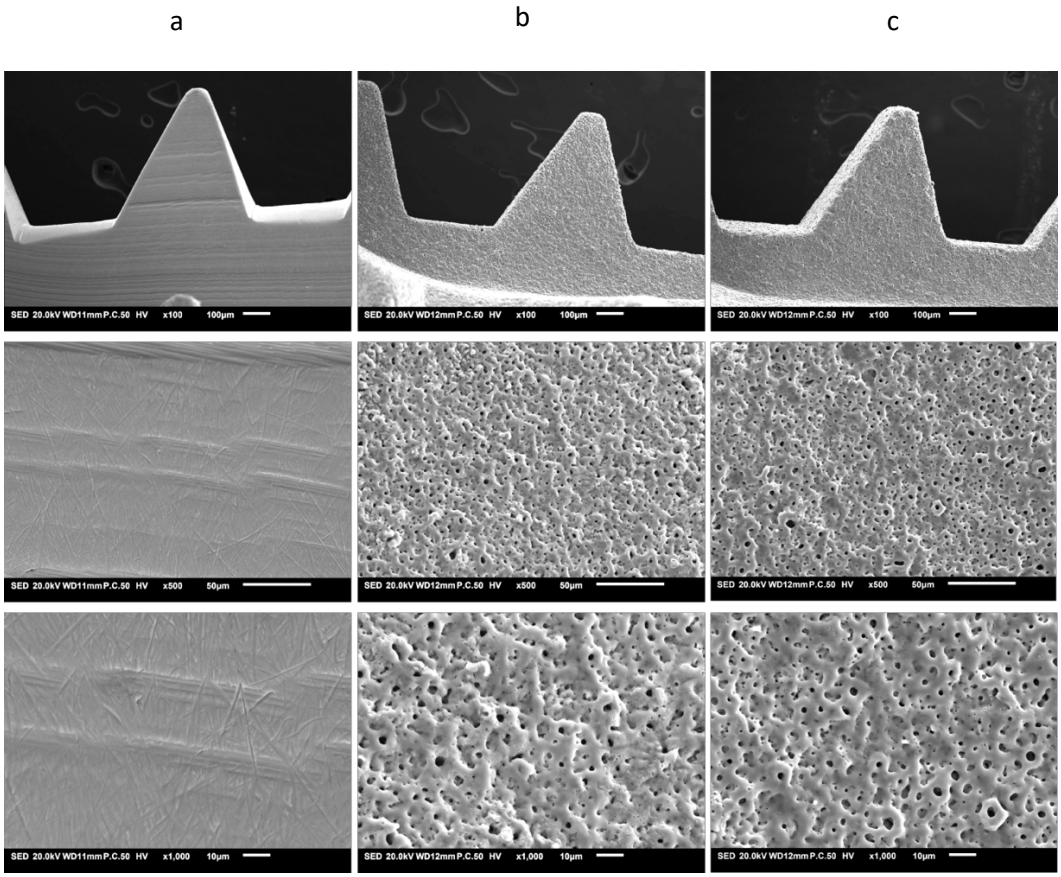

Figure 12: Region 4: Flat part of a thread on the screw-type implant analysed with SEM. (a) non-treated implants. (b) PEO-treated implants. (c) PEO + Ag treated implants.

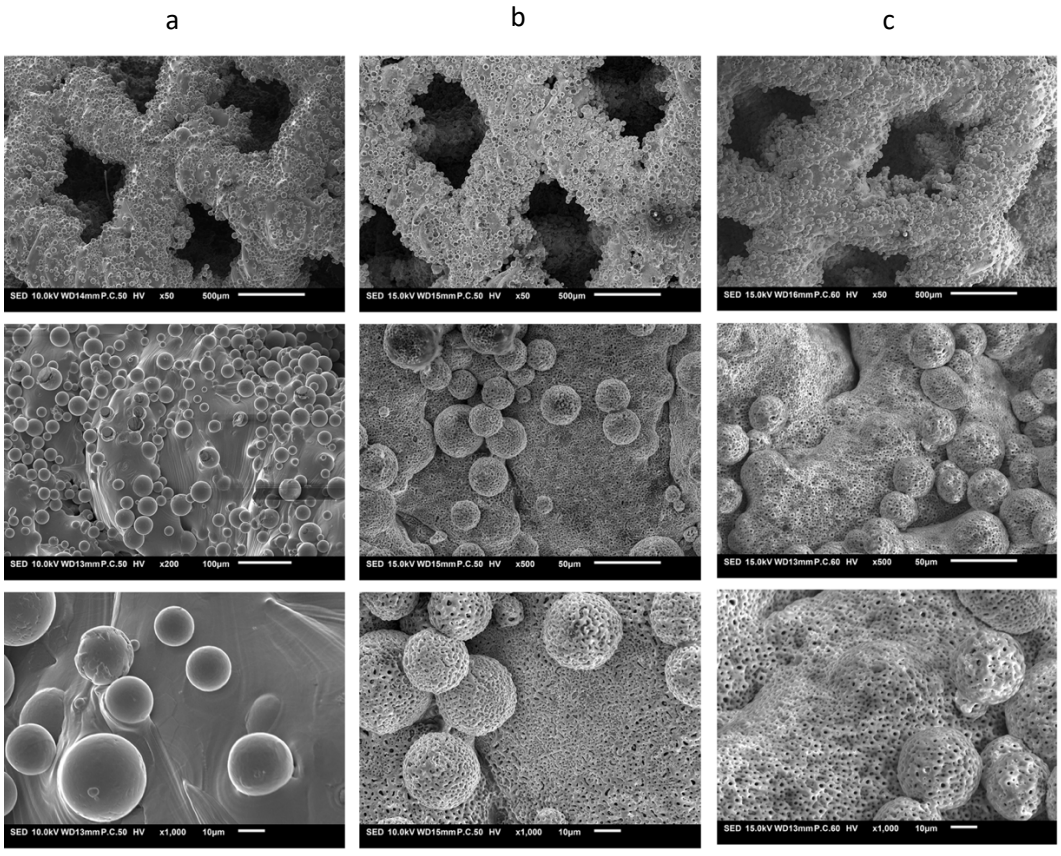

Figure 13: S400 P850 patient-specific implant analysed with SEM. (a) non-treated implants. (b) PEO-treated implants. (c) PEO + Ag treated implants.

3.5 Chemical composition

3.5.1 Screw-type implants

The chemical composition of the titanium oxide layer formed after PEO + Ag on the implant is analysed by SEM and EDS. The identified elements in the layer are: Al, Ti, V, P, O, Ca and Ag. Ti, Al, and V are the alloying elements of the Ti6Al4V implants. The P, Ca and Ag elements are originating from the dissolved ionic species of the PEO electrolyte.

In the case of the PEO with silver nanoparticles to treat the surface, the analysis indicated the presence of silver nanoparticles on the layer. A spot analysis is done to see the elements in the layer on that particular spot of the silver nanoparticle. In Figure 14 arrow 1 indicates agglomerated silver nanoparticle and arrow 2 is pointing at the matrix. Figure 15 shows the EDS matrix in which silver is detected on the spot indicated by arrow 1 and TiO_2 with arrow 2.

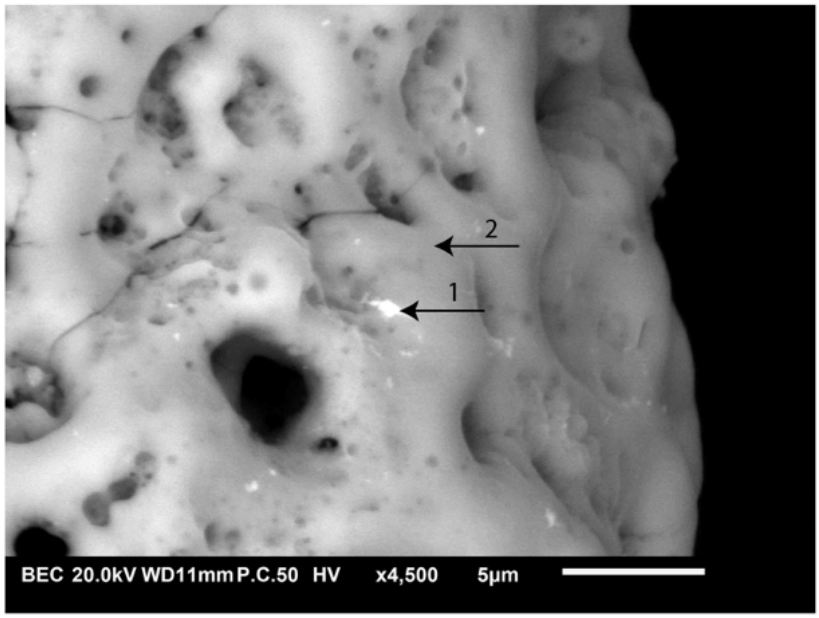

Figure 14: EDS analysis on the PEO + Ag treated implant. Arrow 1 indicates the position of the spot analysis on a silver nanoparticle. Arrow 2 is pointing at the matrix for the spot analysis.

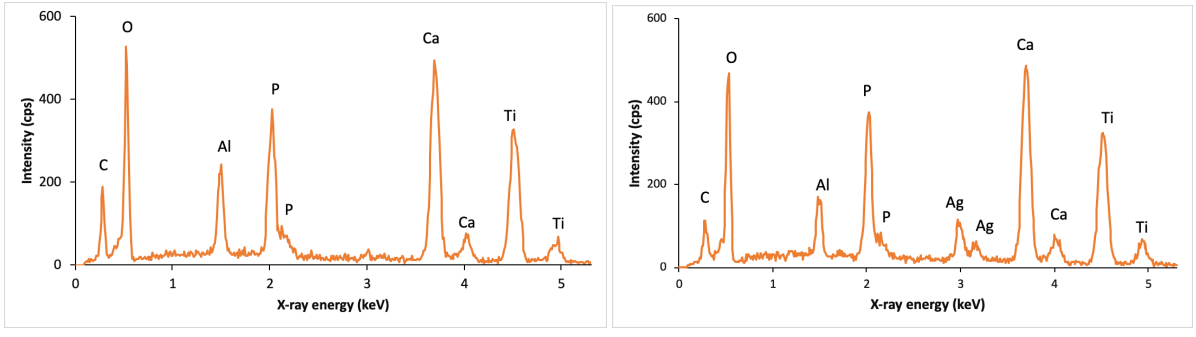

a b

Figure 15: EDS spectrum (a) of matrix and silver particles (b).

3.5.2 Patient-specific implants

On the patient specific additive manufactured implants the silver nanoparticles were identified using SEM with EDS. On all the implants silver nanoparticles are found, equally distributed over the surface area.

In Figure 16 arrow 1 indicates a silver nanoparticle and arrow 2 is pointing at the matrix. Figure 17 show the EDS matrix in which silver is detected on the spot indicated by arrow 1.

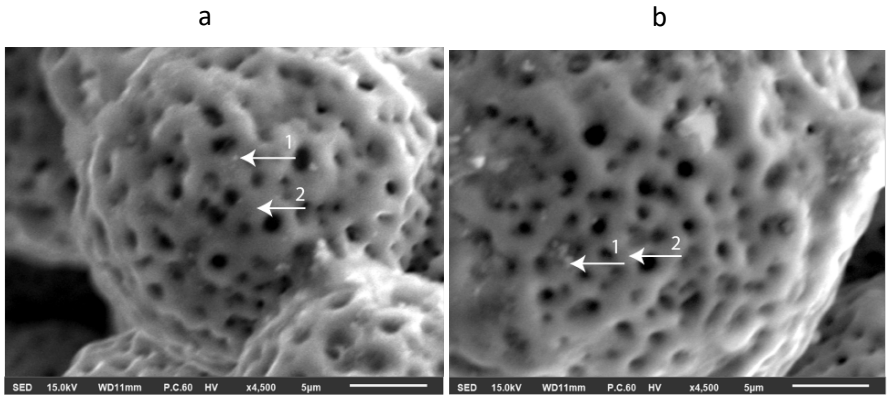

Figure 16: EDS analysis. A. PEO + Ag treated S300 P980 implant. B. PEO + Ag P400 S850. Arrow 1 indicates the position of the spot analysis on a silver nanoparticle. Arrow 2 is pointing at the matrix for the spot analysis.

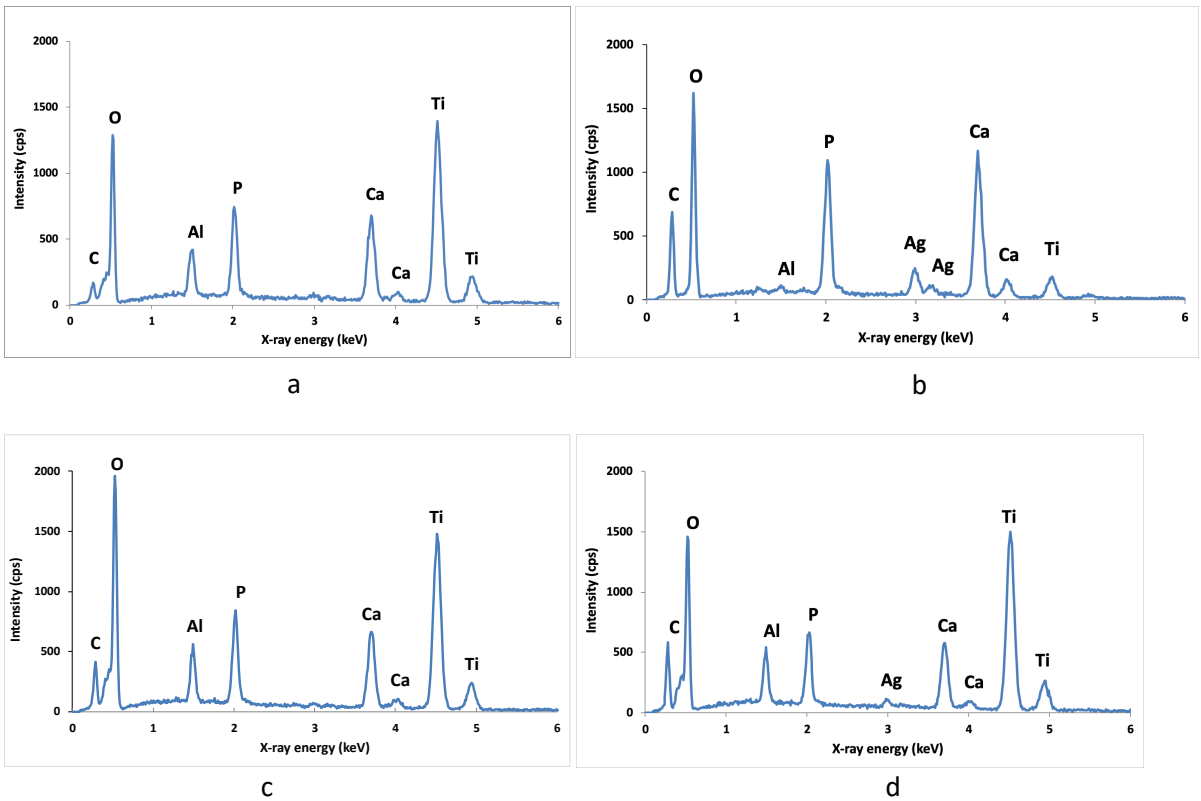

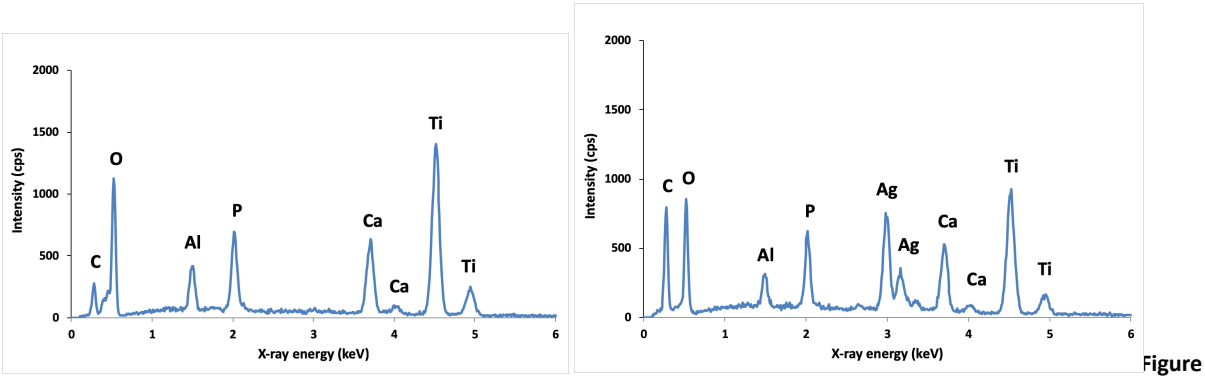

Figure

Figure 17: EDS spectra the samples on the spots as indicated in Figure 13, revealing the presence of Ti, Al, O, P, Ca, Ag elements. (a) S300 P780 TiO_2 matrix (b) S300 P780 Ag (c) S300 P980 TiO_2 matrix (d)) S300 P980 Ag (e) S400 P850 TiO_2 matrix (f)) S400 P850 Ag.

3.6 Phase composition of the layer

The phase composition of the implants was analysed by X-ray diffraction (XRD). As can be seen in Figure 18, the non-treated implants consists of titanium (Ti6Al4V) peaks. The PEO-treated screw-type samples show that next to Ti peaks, TiO_2 rutile phase is present (Figure 18). The PEO- treated patient-specific samples show that the oxide layer consists of titanium and both TiO_2 rutile and anatase phases (Figure 19).

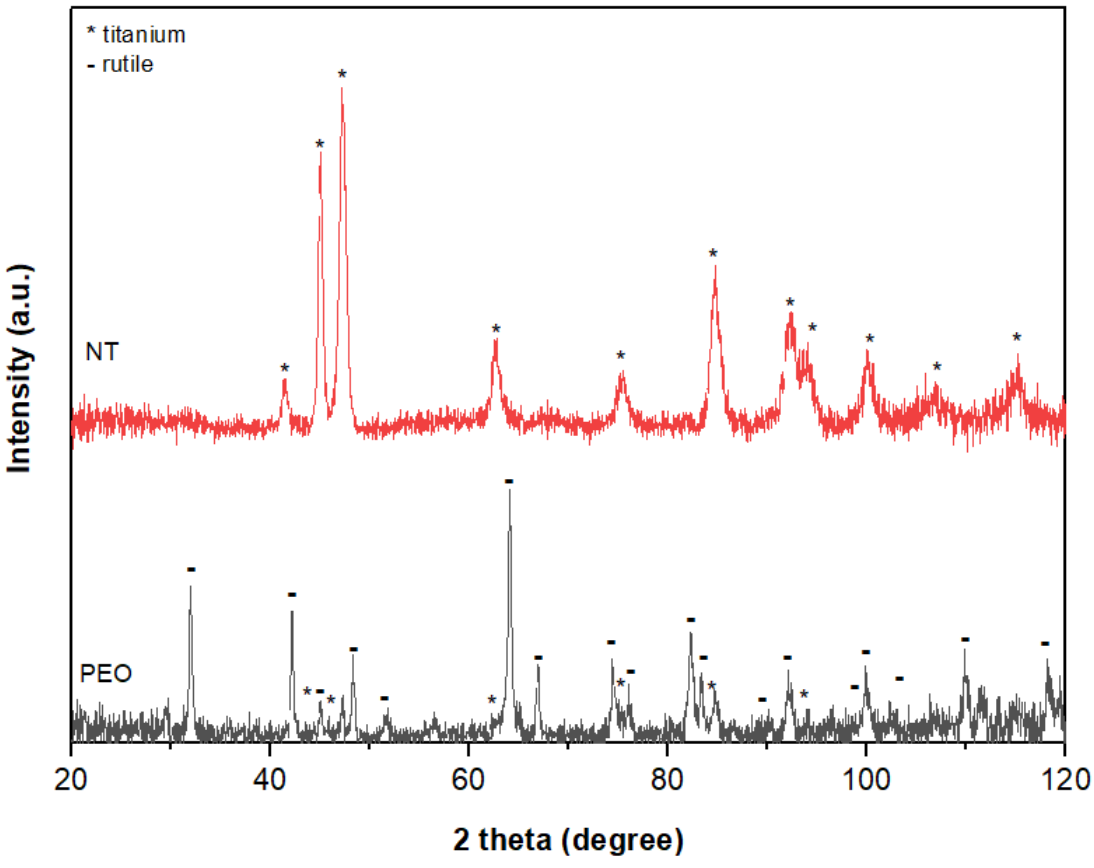

Figure 18: XRD pattern sample screw-type implant.

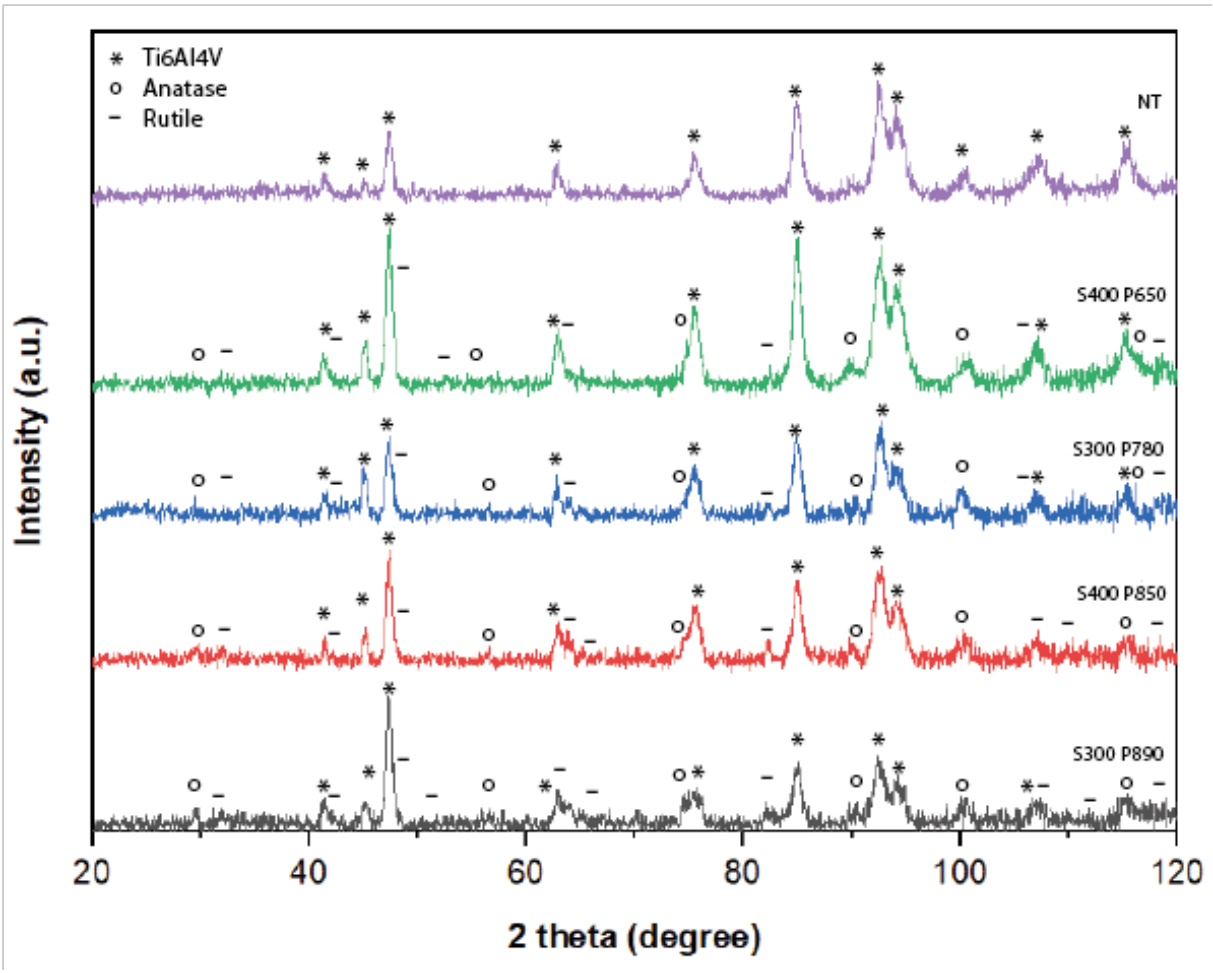

Figure 19: XRD pattern of the PEO-treated patient-specific samples.

3.7 Ion-release

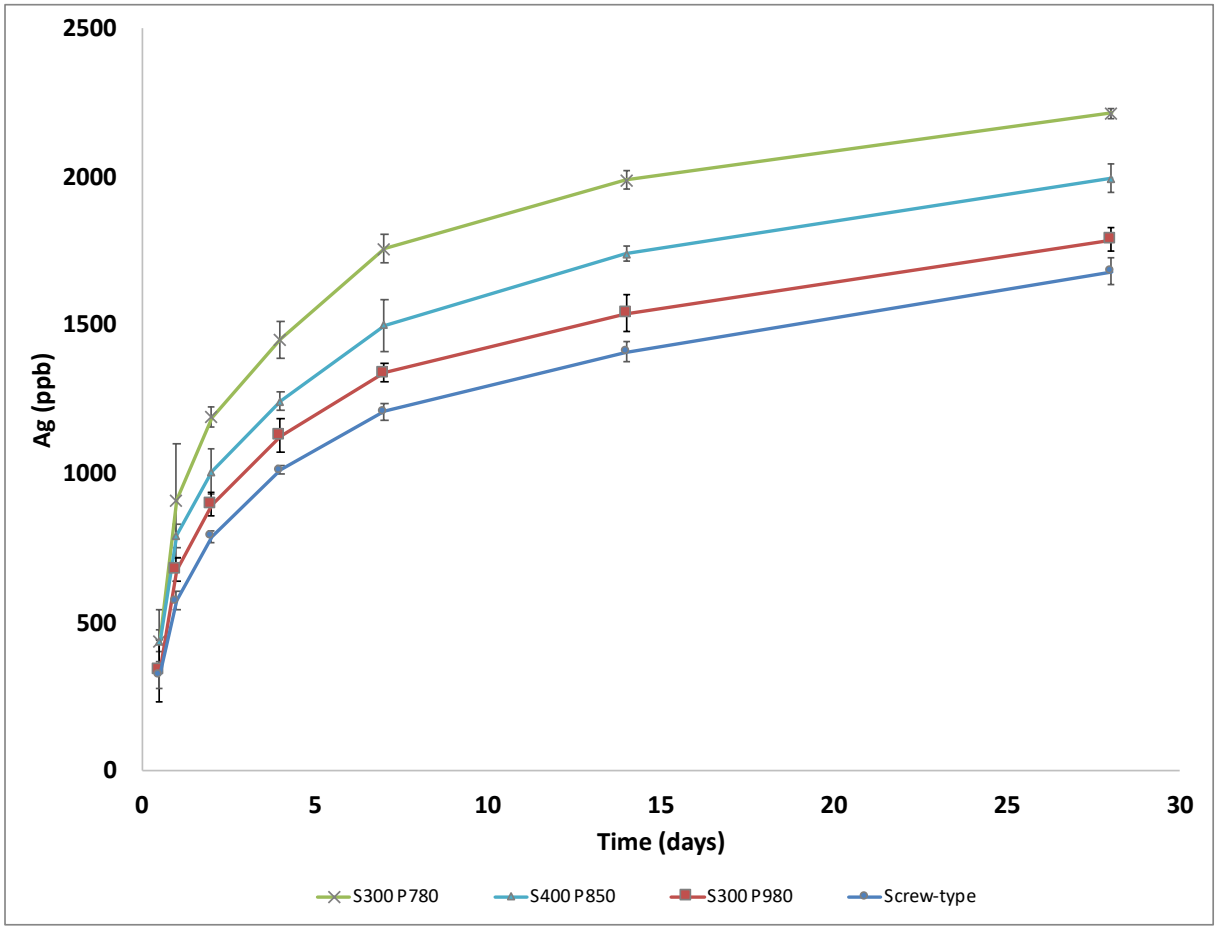

Figure 20: Silver ion release from dental implants. The release of the ions were measured up to 28 days. Cumulative ion release is shown in the graph, including the standard deviation (n=3).

The ion release concentrations of silver were measured using ICP-OES. Measurements took place for one month (28 days). An initial burst release of silver ions was observed after 0.5 day, most silver ions were released in this period. A slower, progressive, release was found after this up to 28 days. The highest ion release is found on the S300 P780 implant (2213.8 ppb), followed by S400 P850 implant (1994.3 ppb), S300 P980 implant (1790.1 ppb) and the screw type implant (1682.8 ppb), respectively (figure 20).

3.8 Zone of inhibition

Antibacterial testing was conducted by putting the implants in contact with MRSA. The inhibition zone was measured around the implants. The area of the zone of inhibition can be found in Figure 21. Earlier studies already indicated a significant difference between PEO-treated implants and PEO + Ag treated implants. In this study only PEO + Ag treated samples are incorporated for this test to compare the different porous implants. The porous implants (S300 P780 and S300 P980) showed a larger zone of inhibition than the screw type implants (Figure 22). A one-way ANOVA test indicated a significant value

between screw type and S300 P780 p<0.05 and between screw-type and S300 P980 p<0.05. No significant difference was found between S300 P780 and S300 P980 p>0.05.

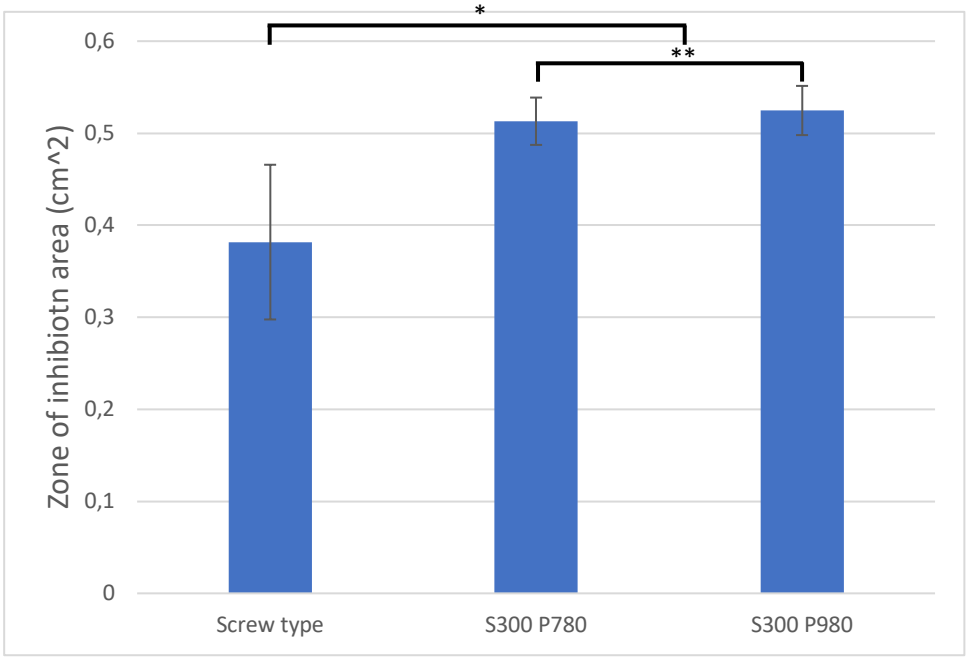

Figure 21: Zone of inhibition of dental implants. This test indicates the zone of inhibition of the dental implants against MRSA. Bars indicated the standard deviation of the results (n=3 for all implants). * p<0.05, **p>0.05.

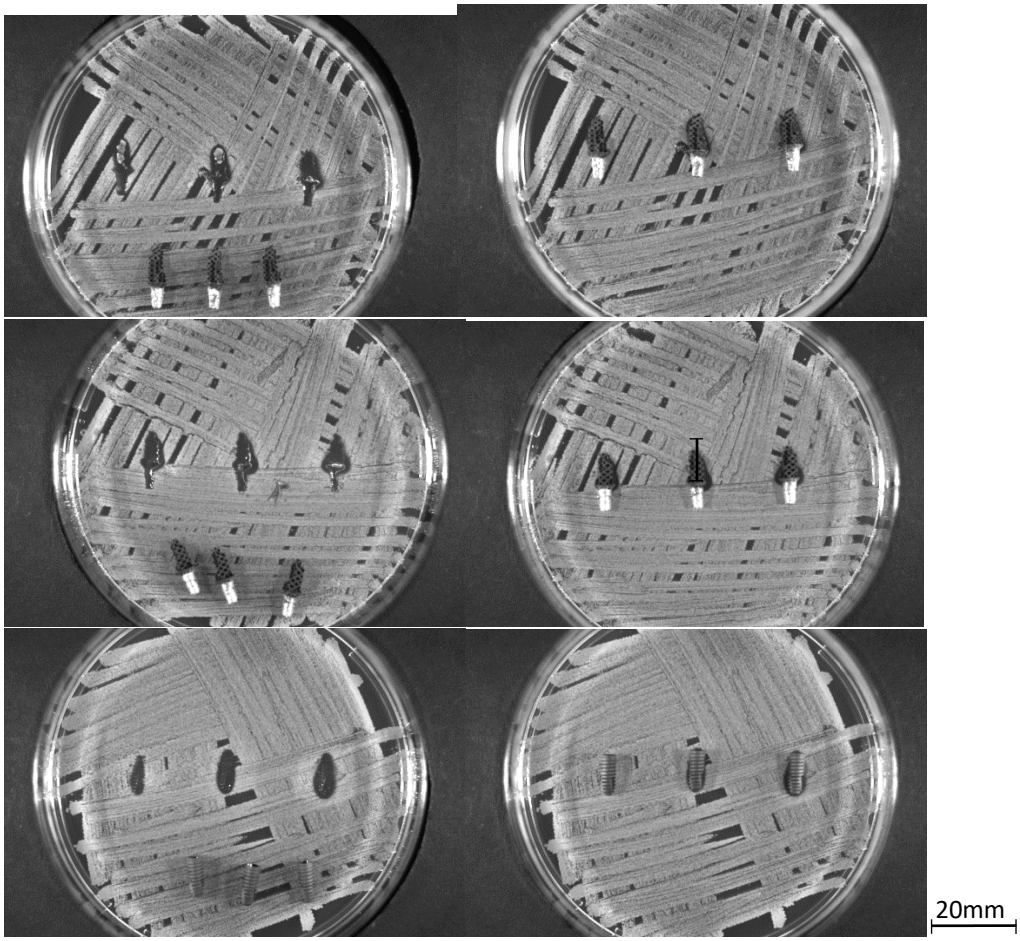

Figure 22: Zone of inhibition of dental implants. This test indicates the zone of inhibition of the dental implants against MRSA. (a) S300 P780 (b)S300 P980 (c) screw-type.

4. Discussion

Dental implants are used to replace teeth. It is a good way to restore function and dental implants have a success rate of 90% [1]. Dental implants can fail by a lack of osseointegration and infection. In this study a new type of dental implants is designed. This new type of implant is a patient-specific, root shaped additive manufactured one. This was created using SLM with Ti6Al4V particles.

Using additive manufacturing techniques, it was possible to create a porous structure. This porous structure was created to improve the osseointegration properties of the implant. By creating a porous structure, the surface area of the dental implant increased. A positive effect of this enlarged area was that bone cells can grow into this structure, and therefore the implant will be better integrated inside the jawbone. However, a negative side effect is that the enlarged surface area can facilitate more bacteria. To overcome bacteria adhesion, an antimicrobial surface was applied on the implants. This surface was created using PEO with silver nanoparticles. These nanoparticles were incorporated in the TiO_2 surface layer that was created during the PEO process.

This study aimed to identify the possibilities of applying an antimicrobial surface on existing screw-type dental implants and the porous patient-specific implants. Four different porosities of the additive manufactured dental implants were created, compared and evaluated with each other.

All surfaces of the implants were successfully treated using the PEO process. The TiO_2 layer was formed homogeneously on all implants. The implants showed a micro/nanoporous surface layer.

Using the zone of inhibition test, it was identified that all implants showed antibacterial activity against MRSA. The ion release test indicated that a higher ion release was found on the additive manufactured dental implants with a higher surface area than the screw-type dental implants.

In this study, patient-specific additive manufactured implants were designed. The design was obtained from a CBCT scan of a real patient. With image segmentation software the exact shape of the root was obtained.

The patient-specific implants created in this study were based on previous studies in which root-analogue implants were discussed. Hodosh et al. [55] created the first root-analogue implants in 1969. This implant was made from polymethacrylate. Unfortunately during the experiments with these type of implants, osseointegration did not take place, instead soft tissue was formed around the implants [55]. Later on root-analogue implants out of titanium were created, which did osseointegrate [33]. A clinical study revealed good primary stability, but a high failure rate after nine months (48%) because of incongruence between implant and socket. Nowadays, it is possible to use CBCT scanning equipment, CAD and printing technologies to create root-analogue-implants with more precision than before[28]. This allows the fabrication of dental implants that are mimicking the shape of the original root. In the study of Figliuzzi et al [29], they created a root-analogue implant with these technologies, which resulted in a good functional and esthetic integration.

In this study, CBCT scanning, CAD software 3DXpert and SLM printing were used to create porous patient-specific root shaped implants. The results showed the ability of creating complex porous geometries to create patient-specific root shaped dental implants. Which was also shown in studies of Peng et al. [56].

First these implants were printed with an FDM printer (3x scaled up) to test the concept of patient-specific implants (Figure 6). It became clear that the implant needed to be scaled down in an x or y direction to fit in the socket. After a scaling of down of 0.1 in either x or y direction the implant did fit

in the socket. This proves the main principle of this patient-specific-dental-implant-concept: a dental root can be scanned, printed and inserted into the exact same socket.

The dimensions of the digital STL files of the porous implants were compared with the dimensions of the non-porous root shape from the CBCT scan (Figure 5). Compared with the original root, the shape of the porous implant was different. This was mainly due to the use of only whole cells in the design. Only whole cells were used because this was easier for the printing, because of the self-supporting structure. If there would be incomplete cells, more support material was needed and this was difficult and time-consuming to remove. By making use of only whole cells the shape was slightly changed. The deviation could also be the result of smoothening and noise reduction during scanning, modelling and printing. The design of the implants was limited by SLM parameters.

The optimal pore size of porous dental implants and orthopedic implants is not known yet. Several studies reported different values [57-59]. Pore sizes of 100-400 µm are able to support the formation of bone tissue inside the pores according to Karageorgiou et al. [57] and Ripamonti [58]. However, in the study by Wang et al. [59] a pore size of 700µm was realized. These dental implants with a porous structure were inserted in the tibia of rabbits and using micro CT scans it was confirmed that bone was grown into the pores and bone was interconnected with the porous structure of the implant.

The parameters of the SLM printer constrained the design of the pore size and strut thickness. The deviation from several porosities, by changing the strut thickness and pore size, was analysed. A smaller porosity resulted in lower deviations from the original root shape (Table 4). Small deviations are preferred, since this would then perfectly fit in the extraction socket. However due to limitations of the SLM process, larger pores had to be printed. Designs with small pores in the STL files, resulted in closed pores after printing, which was not desired (Figure 8). Further developments and optimization of the SLM printer might result in more accurate shapes of the dental implants. So, in this study several relatively large porosities were created which were in between pore sized of 650 and 980 µm. In this study no osseointegration experiments were conducted.

After printing the dimensions of the struts and pores of the printed implants were compared with the dimensions of the STL files of the implants. The designed pore size deviated from the actual dimensions of the manufactured pores (Table 5). The pores were maximumly 200 µm smaller and maximumly 20 µm larger than in the STL file. These findings did relate with findings in the study of Peng et al. in which they identified a deviation around 10 µm on a pore size of 290 and 390 µm [56]. In a study by Moin et al. [54] a mean variation between printed implants and STL file of 15-20 µm was found. This deviation is smaller than the deviations found in this study, this can be due to the parameter settings and type SLM printer used.

Peng et al. identified that the decrease in pore size did not have an influence in the osseointegration results. They revealed that bone tissue could grow and penetrate into the porous dental implant structure (tested in rabbit limbs) by CT scanning and histological analysis [56]. They also analyzed the bonding strength of these porous implants by push out and torque testing. They identified that porous implants were stronger than solid screw-type implants, since bone tissue was penetrated through the porous structure and was bounded tightly to the struts of the implant [56].

Successful osseointegration is also linked to primary stability of the implant [60]. Screw-type implants obtain their primary stability by screw retaining in the socket [61]. Primary stability of root-analogue implants is achieved through a good congruence between implant and socket, which can be achieved by pressurized fit, adding macro and micro-retentions with supportive surface modifications [26], [55–57]. It has been shown that porous surfaces are more osteoconductive than surfaces that are smooth [58, 59]. Increased roughness, leads to enlarged surface areas, leading to improved cell

migration and attachment, growing of bone tissue inside the pores, enhancing osseointegration, better fixation [60, 61].

The macro porous structure and the micro/nano porosity due to PEO will add to this primary stability. However, osseointegration properties of these structures were not evaluated.

The rough surfaces are thus beneficial for osseointegration, however this rough surface has also an increased surface area onto which bacteria can adhere. At this moment, no dental implants with antibacterial properties are commercially available. In this study the dental implants, both screw-type and patient-specific, were surface treated to create antibacterial implants. This way the proposed design of the patient-specific implant in this study, consisted of a porous structure with a rough surface to promote osseointegration, including silver nanoparticles to overcome bacterial infections.

The dental implants were PEO processed after the SLM printing. PEO was used to create the antimicrobial layer on the surface. PEO was used in previous studies in which complex shapes additive manufactured implants were successfully surface treated with this method in a single step process [62–64].

The surface of the Ti6Al4V dental implants have a thin natural TiO_2 layer [72]. During this process, oxidation-reduction reaction cause thickening of the TiO_2 layer on the surface. A dielectric breakdown causes sparks forming a porous TiO_2 layer in which electrolyte compounds and the nanoparticles are incorporated in the layer. The TiO_2 layers grows inwards and outwards which creates a strong adhesion with the implants. This created porous layer is rough and supports the osseointegration properties of the implants [73].

The parameters that are used for the PEO process were 20A/dm^2 for 300 sec. This was based on previous studies [62–64]. After PEO, the implants were analyzed with SEM and this showed that the surface layer was turned into a micro/nanoporous layer (Figures 12 and 13). The morphology of the implant surfaces were in accordance with other studies done on PEO-treated Ti6Al4V implants with similar electrolytes [62, 67].

The V-t curves of the PEO process showed similar behavior for all implants except the S400 P650. Between the other implants only a small deviation between breakdown voltages was observed, as well as small differences between PEO with and without silver. However, this did not have an influence on the surface morphology of the implants. The difference in voltage until breakdown were probably related to the electrolyte conductivity. Due to the silver nanoparticles in the electrolyte the conductivity increased, which resulted in less resistant and eventually a thinner oxide layer. A higher melting temperature will lead to a higher breakdown voltage. On the S400 P650 porosity AM implant, the PEO process including silver particles did not succeed. The reason for this could be that there was a damage in the struts, causing the current not completely flow through the entire structure.

Silver nanoparticles were added because of its antibacterial properties. The presence of the silver nanoparticles in the TiO_2 layer was confirmed using SEM with EDS. Other elements in the layer were Ti, Al, (from the Ti6Al4V alloy), Ca, P (from the calcium glycerophosphate and calcium acetate electrolyte), and O. In a previous study results indicated that the PEO morphology on the implant with Ca and P elements stimulate bone regeneration and bone integration in relation to implants that were not surface treated with PEO [69, 70].

During the PEO process the high temperatures of the plasma discharges supported crystallization of the amorphous TiO_2 layer into rutile and anatase phases [71, 72]. The phase composition of the TiO_2 layer was identified with XRD. The XRD experiments on the implants indicated that a TiO_2 layer was formed on the implants, containing rutile and anatase phases. On the screw-type dental implants no anatase phase was identified. Only rutile titanium dioxide was identified by the XRD. The samples had relatively large holes and complex geometries, which made it difficult for the detector to be positioned in the right spot. According to Gaintantzopoulou et al., it is difficult to apply an XRD analysis on commercially available implants, because of the complex 3D morphology and of poor spatial resolution related to XRD [79]. XRD is also prone to fail to analyze precisely arc-oxidized titanium surfaces, because of minimal thickness of the layer and reduced crystallinity [80]. Arc-oxidized implants are known to have anatase [75–77]. Rutile can be identified next to anatase, when a higher voltage is used during oxidation [84]. Anatase is associated with improved biological activity, related to osteoblast adhesion, spreading, proliferation and differentiation [85]. It has less corrosion resistant properties than rutile. In the study conducted by Van Hengel et al. [69], mainly rutile phase was found after PEO on the 3D printed Ti6Al4V implants used in the study.

Reactive oxygen species can be caused by the rutile and anatase phases in the TiO_2 layer [86]. ROS can induce stress in the bacterial cell and damage the DNA resulting in cell death [81–87].

Another aspect of the antibacterial activity of the implants was created by adding silver nanoparticles during the PEO process. Silver has shown to have antibacterial activity against peri-implantitis. In a pre-clinical study by Gallardo et al. [94] dental implants with silver nanoparticles (silver electrodeposition) were placed in the mandible of dogs and peri-implantitis was induced two months later. Bone resorption was higher in the non-treated implant cases, showing that antibacterial treatments with silver nanoparticles have a positive influence against bone resorption after inducing peri-implantitis [94].

Antimicrobial effect of the surface was evaluated in vitro experiments; a zone of inhibition test and an ion release test.

Due to the leaching activity of the silver ions a clear zone of inhibition was identified. Previous studies have indicated no clear growth inhibition zone around implants without silver nanoparticles [69]. The results of this study do not clearly indicate a relation between surface area and dimensions of the zone of inhibition. The total area of the zone of inhibition was smaller, since the bacteria were taken from the fridge, and therefore they grew less fast. The difference between the surface areas of the implants with different porosities (S300 P780 and S300 P980) did not result in a significant different zone of inhibitions. The reason for this could be that the surface area that was placed in the agar was different. This could not be controlled. The implants have a different geometry, which might resulted in more area touching the agar from the S300 P780 implants than from the S300 P980 implants.

During the ion release test the implants were placed in PBS for 28 days. For all implants an initial burst release in the first 12 hours was identified, thereafter the release persisted up to 28 days. This burst release was also observed by Pokrowiecki et al., [89] Mei et al.,[90] and Unosson et al. [91]. The burst release of silver ions in the first 12 hours will lead to a high concentration of antibacterial agents around the implant over a short period of time. This burst release is needed to prevent the adhesion of bacteria on the surface at the early stage after implantation. The initial burst release was also found in similar studies with silver nanoparticles by Van Hengel et al. and Putra et al. [62, 64].

The implants with a larger surface area released higher concentrations of ions compared to the implants with smaller surface areas. The screw-type implant had the smallest surface area and

released less silver ions compared to all porous implants. The concentration of silver ions releases was related to the surface area of the implants. The implant with the highest surface area (S300 P780) released cumulatively 2213.8 ppb ions, followed by the S400 P850 implant and S300 P980 implant and the lowest amount was released from the screw-type implants. These data indicate that a larger surface area results in a higher release of silver ions, probably because more silver nanoparticles are incorporated in the TiO_2 layer. This is also in agreement with a previous study conducted by Van Hengel et al [69], who studied solid and 3D printed porous implants.

The total amount of silver ions after 24 hours was 0.91 ppm for S300 P780, 0.80 ppm for S400 P850, 0.68ppm for S300 P980 and 0.57ppm for the screw-type implants.

Oral biofilm involves many bacterial species, more than 700 different ones [98]. In this study the antibacterial activity of the implants was only tested against MRSA. Therefore, it is important to do further testing with other bacteria species too. In vitro oral multispecies biofilm models are developed to be used for testing [93–95]. For dental implants effective preventive behavior is important to have antibacterial properties against bacteria that cause peri-implantitis.

5. Conclusions

In this study a novel approach to create patient-specific dental implants with a porous structure to promote osseointegration and with an antimicrobial surface to prevent infection is proposed. With the currently available techniques, such as CBCT scans, CAD programs and SLM printing of titanium, it is already feasible to create these type of implants. A next step in the development of root-analogue implants is taken. The combination of root-shaped implants with a porous structure provides a way to shorten the implant procedure by immediate placement after tooth extraction. The root-shaped implant allows this and the porous structure will be advantageous for osseointegration and stability of the implant.

Due to the increased surface area, it is important to create an antimicrobial surface. In previous studies this has been researched, but not intensively on dental implants. Here silver nanoparticles are incorporated using the PEO process to create antimicrobial surfaces on the implants. Silver is known to have antibacterial activity, which is also identified in this study. The implants showed antibacterial activity against MRSA. The silver ion release of the implants was identified too. The porous implants showed a larger zone of inhibition and a higher release of silver ions compared to the screw-type implants. These results are in line with previous studies. The results show great potential to be developed further to enrich the dental implant industry.

6. References

[1] J. Lindhe and J. Meyle, "Peri-implant diseases: Consensus Report of the Sixth European Workshop on Periodontology," *J. Clin. Periodontol.*, vol. 35, no. SUPPL. 8, pp. 282–285, 2008.

[2] J. Derks and C. Tomasi, "Peri-implant health and disease. A systematic review of current epidemiology," *J. Clin. Periodontol.*, vol. 42, no. S16, pp. S158–S171, 2015.

[3] H. Algraffee, F. Borumandi, and L. Cascarini, "Peri-implantitis," *Br. J. Oral Maxillofac. Surg.*, vol. 50, no. 8, pp. 689–694, 2012.

[4] N. Broggini *et al.*, "Peri-implant inflammation defined by the implant-abutment interface," *J. Dent. Res.*, vol. 85, no. 5, pp. 473–478, 2006.

[5] Y. C. M. De Waal, A. J. Van Winkelhoff, H. J. A. Meijer, G. M. Raghoebar, and E. G. Winkel, "Differences in peri-implant conditions between fully and partially edentulous subjects: A systematic review," *J. Clin. Periodontol.*, vol. 40, no. 3, pp. 266–286, 2013.

[6] I. K. Karoussis, S. Müller, G. E. Salvi, L. J. A. Heitz-Mayfield, U. Brägger, and N. P. Lang, "Association between periodontal and peri-implant conditions: A 10-year prospective study," *Clin. Oral Implants Res.*, vol. 15, no. 1, pp. 1–7, 2004.

[7] U. Brägger, I. Karoussis, R. Persson, B. Pjetursson, G. Salvi, and N. P. Lang, "Technical and biological complications/failures with single crowns and fixed partial dentures on implants: A 10-year prospective cohort study," *Clin. Oral Implants Res.*, vol. 16, no. 3, pp. 326–334, 2005.

[8] P. Simonis, T. Dufour, and H. Tenenbaum, "Long-term implant survival and success: A 10-16-year follow-up of non-submerged dental implants," *Clin. Oral Implants Res.*, vol. 21, no. 7, pp. 772–777, 2010.

[9] M. Hultin, A. Gustafsson, H. Hallström, L. Å. Johansson, A. Ekfeldt, and B. Klinge, "Microbiological findings and host response in patients with peri-implantitis," *Clin. Oral Implants Res.*, vol. 13, no. 4, pp. 349–358, 2002.

[10] S. Chen and I. Darby, "Dental implants: Maintenance, care and treatment of peri-implant infection," *Aust. Dent. J.*, vol. 48, no. 4, pp. 212–220, 2003.

[11] A. Leonhardt, S. Renvert, and G. Dahlén, "Microbial findings at failing implants," *Clin. Oral Imp. Res.*, vol. 10, no. 3. pp. 339–345, 1999.

[12] M. A. Sánchez-Gárces and C. Gay-Escoda, "Periimplantitis.," *Med. Oral Patol. Oral Cir. Bucal*, vol. 9 Suppl, no. 1, 2004.

[13] S. Sharma *et al.*, "Silk fibroin nanoparticles support in vitro sustained antibiotic release and osteogenesis on titanium surface," *Nanomedicine Nanotechnology, Biol. Med.*, vol. 12, no. 5, pp. 1193–1204, 2016.

[14] Y. Cheng *et al.*, "Fabrication and in vitro release behavior of a novel antibacterial coating containing halogenated furanone-loaded poly(L-lactic acid) nanoparticles on microarc-oxidized titanium," *Int. J. Nanomedicine*, vol. 7, pp. 5641–5652, 2012.

[15] E. H. Abdulkareem, K. Memarzadeh, R. P. Allaker, J. Huang, J. Pratten, and D. Spratt, "Anti-biofilm activity of zinc oxide and hydroxyapatite nanoparticles as dental implant coating materials," *J. Dent.*, vol. 43, no. 12, pp. 1462–1469, 2015.

[16] T. Berglundh, N. U. Zitzmann, and M. Donati, "Are peri-implantitis lesions different from

periodontitis lesions?," *J. Clin. Periodontol.*, vol. 38, no. SUPPL. 11, pp. 188–202, 2011.

[17] D. Lebeaux, J.-M. Ghigo, and C. Beloin, "Biofilm-Related Infections: Bridging the Gap between Clinical Management and Fundamental Aspects of Recalcitrance toward Antibiotics," *Microbiol. Mol. Biol. Rev.*, vol. 78, no. 3, pp. 510–543, 2014.

[18] L. Hall-Stoodley and P. Stoodley, "Evolving concepts in biofilm infections," *Cell. Microbiol.*, vol. 11, no. 7, pp. 1034–1043, 2009.

[19] W. Orapiriyakul, P. S. Young, L. Damiati, and P. M. Tsimbouri, "Antibacterial surface modification of titanium implants in orthopaedics," *J. Tissue Eng.*, vol. 9, 2018.

[20] R. P. Allaker, "Critical review in oral biology & medicine: The use of nanoparticles to control oral biofilm formation," *J. Dent. Res.*, vol. 89, no. 11, pp. 1175–1186, 2010.

[21] J. Huang, X. Li, G. P. Koller, L. Di Silvio, M. A. Vargas-Reus, and R. P. Allaker, "Electrohydrodynamic deposition of nanotitanium doped hydroxyapatite coating for medical and dental applications," *J. Mater. Sci. Mater. Med.*, vol. 22, no. 3, pp. 491–496, 2011.

[22] B. S. Atiyeh, M. Costagliola, S. N. Hayek, and S. A. Dibo, "Effect of silver on burn wound infection control and healing: Review of the literature," *Burns*, vol. 33, no. 2, pp. 139–148, 2007.

[23] K. Li, Y. Xie, L. Huang, H. Ji, and X. Zheng, "Antibacterial mechanism of plasma sprayed Ca2ZnSi 2O7 coating against Escherichia coli," *J. Mater. Sci. Mater. Med.*, vol. 24, no. 1, pp. 171–178, 2013.

[24] L. Rizzello and P. P. Pompa, "Nanosilver-based antibacterial drugs and devices: Mechanisms, methodological drawbacks, and guidelines," *Chem. Soc. Rev.*, vol. 43, no. 5, pp. 1501–1518, 2014.

[25] C. E. Kazor, K. Al-Shammari, D. P. Sarment, C. E. Misch, and H. Wang, "Implant plastic surgery: review and rationale," *J Oral Implantol.*, vol. XXX, no. 4, pp. 240–254, 2004.

[26] R. U. Koh, I. Rudek, and H. L. Wang, "Immediate implant placement: Positives and negatives," *Implant Dent.*, vol. 19, no. 2, pp. 98–108, 2010.

[27] K. M. Regish, D. Sharma, and M. D. R. Prithviraj, "An Overview of Immediate Root Analogue Zirconia Implants," *J. Oral Implantol.*, vol. 29, no. 2, pp. 225–233, 2013.

[28] D. A. Moin, B. Hassan, P. Mercelis, and D. Wismeijer, "Designing a novel dental root analogue implant using cone beam computed tomography and CAD/CAM technology," *Clin. Oral Implants Res.*, vol. 24, no. A100, pp. 25–27, Aug. 2013.

[29] M. Figliuzzi, F. Mangano, and C. Mangano, "A novel root analogue dental implant using CT scan and CAD/CAM: selective laser melting technology.," *Int. J. Oral Maxillofac. Surg.*, vol. 41, no. 7, pp. 858–862, Jul. 2012.

[30] F. G. Mangano, B. Cirotti, R. L. Sammons, and C. Mangano, "Custom-made, root-analogue direct laser metal forming implant: a case report," *Lasers Med. Sci.*, vol. 27, no. 6, pp. 1241–1245, Nov. 2012.

[31] C. Mangano, M. Raspanti, T. Traini, A. Piattelli, and R. Sammons, "Stereo imaging and cytocompatibility of a model dental implant surface formed by direct laser fabrication," *J. Biomed. Mater. Res. Part A*, vol. 88A, no. 3, pp. 823–831, Mar. 2009.

[32] T. Traini, C. Mangano, R. L. Sammons, F. Mangano, A. Macchi, and A. Piattelli, "Direct laser metal sintering as a new approach to fabrication of an isoelastic functionally graded material

for manufacture of porous titanium dental implants," *Dent. Mater.*, vol. 24, no. 11, pp. 1525–1533, Nov. 2008.

[33] D. Lundgren, H. Rylander, M. Anderssong, C. Johansson, and T. Albrektsson, "Healing-in of root analogue titanium implants placed in extraction sockets. An experimental study in the beagle dog.," *Clin. Oral Implants Res.*, vol. 3, no. 3, pp. 136–144, Sep. 1992.

[34] R.-J. Kohal, M. B. Hurzeler, L. F. Mota, G. Klaus, R. G. Caffesse, and J. R. Strub, "Custom-made root analogue titanium implants placed into extraction sockets. An experimental study in monkeys.," *Clin. Oral Implants Res.*, vol. 8, no. 5, pp. 386–392, Oct. 1997.

[35] W. Pirker and A. Kocher, "Immediate, non-submerged, root-analogue zirconia implants placed into single-rooted extraction sockets: 2-year follow-up of a clinical study.," *Int. J. Oral Maxillofac. Surg.*, vol. 38, no. 11, pp. 1127–32, Nov. 2009.

[36] W. Pirker, D. Wiedemann, A. Lidauer, and A. A. Kocher, "Immediate, single stage, truly anatomic zirconia implant in lower molar replacement: a case report with 2.5 years follow-up.," *Int. J. Oral Maxillofac. Surg.*, vol. 40, no. 2, pp. 212–6, Feb. 2011.

[37] G. E. Ryan, A. S. Pandit, and D. P. Apatsidis, "Porous titanium scaffolds fabricated using a rapid prototyping and powder metallurgy technique," *Biomaterials*, vol. 29, no. 27, pp. 3625–3635, Sep. 2008.

[38] M. Koike, K. Martinez, L. Guo, G. Chahine, R. Kovacevic, and T. Okabe, "Evaluation of titanium alloy fabricated using electron beam melting system for dental applications," *J. Mater. Process. Technol.*, vol. 211, no. 8, pp. 1400–1408, 2011.

[39] G. Ryan, A. Pandit, and D. P. Apatsidis, "Fabrication methods of porous metals for use in orthopaedic applications," *Biomaterials*, vol. 27, no. 13, pp. 2651–2670, 2006.

[40] N. Taniguchi *et al.*, "Effect of pore size on bone ingrowth into porous titanium implants fabricated by additive manufacturing: An in vivo experiment," *Mater. Sci. Eng. C*, vol. 59, pp. 690–701, Feb. 2016.

[41] A. A. Zadpoor, "Bone tissue regeneration: The role of scaffold geometry," *Biomater. Sci.*, vol. 3, no. 2, pp. 231–245, 2015.

[42] Y. Kuboki, Q. Jin, and H. Takita, "Geometry of carriers controlling phenotypic expression in BMP-induced osteogenesis and chondrogenesis.," *J Bone Jt. Surg*, vol. 83, no. A, pp. 105–115, May 2001.

[43] S. M. Ahmadi *et al.*, "Additively manufactured open-cell porous biomaterials made from six different space-filling unit cells: The mechanical and morphological properties," *Materials (Basel).*, vol. 8, no. 4, pp. 1871–1896, 2015.

[44] M. A. Lopez-Heredia *et al.*, "Bone growth in rapid prototyped porous titanium implants," *J. Biomed. Mater. Res. - Part A*, vol. 85, no. 3, pp. 664–673, 2008.

[45] L. Mullen, R. C. Stamp, W. K. Brooks, E. Jones, and C. J. Sutcliffe, "Selective laser melting: A regular unit cell approach for the manufacture of porous, titanium, bone in-growth constructs, suitable for orthopedic applications," *J. Biomed. Mater. Res. - Part B Appl. Biomater.*, vol. 89, no. 2, pp. 325–334, 2009.

[46] K. Memarzadeh, A. S. Sharili, J. Huang, S. C. F. Rawlinson, and R. P. Allaker, "Nanoparticulate zinc oxide as a coating material for orthopedic and dental implants," *J. Biomed. Mater. Res. Part A*, vol. 103, no. 3, pp. 981–989, 2015.

[47] Y. Yu, G. Jin, Y. Xue, D. Wang, X. Liu, and J. Sun, "Multifunctions of dual Zn/Mg ion co-

implanted titanium on osteogenesis, angiogenesis and bacteria inhibition for dental implants," *Acta Biomater.*, vol. 49, pp. 590–603, 2017.

[48] S. Qiao *et al.*, "Ag-plasma modification enhances bone apposition around titanium dental implants: An animal study in labrador dogs," *Int. J. Nanomedicine*, vol. 10, pp. 653–664, 2015.

[49] M. A. Massa *et al.*, "Synthesis of new antibacterial composite coating for titanium based on highly ordered nanoporous silica and silver nanoparticles," *Mater. Sci. Eng. C*, vol. 45, pp. 146–153, 2014.

[50] B. S. Necula, I. Apachitei, L. E. Fratila-Apachitei, E. J. Van Langelaan, and J. Duszczyk, "Titanium bone implants with superimposed micro/nano-scale porosity and antibacterial capability," *Appl. Surf. Sci.*, vol. 273, pp. 310–314, 2013.

[51] F. G. Mangano, M. De Franco, A. Caprioglio, A. Macchi, A. Piattelli, and C. Mangano, "Immediate, non-submerged, root-analogue direct laser metal sintering (DLMS) implants: a 1-year prospective study on 15 patients," *Lasers Med. Sci.*, vol. 29, no. 4, pp. 1321–1328, Mar. 2013.

[52] J. Chen, Z. Zhang, X. Chen, C. Zhang, G. Zhang, and Z. Xu, "Design and manufacture of customized dental implants by using reverse engineering and selective laser melting technology.," *J. Prosthet. Dent.*, vol. 112, no. 5, pp. 1088–1095, Nov. 2014.

[53] D. Anssari Moin, B. Hassan, and D. Wismeijer, "A novel approach for custom three-dimensional printing of a zirconia root analogue implant by digital light processing," *Clin. Oral Implants Res.*, vol. 28, no. 6, pp. 668–670, Jun. 2017.

[54] D. A. Moin, B. Hassan, A. Parsa, P. Mercelis, and D. Wismeijer, "Accuracy of preemptively constructed, Cone Beam CT-, and CAD/CAM technology-based, individual Root Analogue Implant technique: An in vitro pilot investigation," *Clin. Oral Implants Res.*, vol. 25, no. 5, pp. 598–602, May 2014.

[55] M. Hodosh, M. Povar, and G. Shklar, "The dental polymer implant concept," *J. Prosthet. Dent.*, vol. 22, no. 3, pp. 371–380, 1969.

[56] W. Peng, L. Xu, J. You, L. Fang, and Q. Zhang, "Selective laser melting of titanium alloy enables osseointegration of porous multi-rooted implants in a rabbit model," *Biomed. Eng. Online*, vol. 15, no. 1, pp. 1–13, 2016.

[57] V. Karageorgiou and D. Kaplan, "Porosity of 3D biomaterial scaffolds and osteogenesis," *Biomaterials*, vol. 26, no. 27, pp. 5474–5491, 2005.

[58] U. Ripamonti, "Soluble, insoluble and geometric signals sculpt the architecture of mineralized tissues," *J. Cell. Mol. Med.*, vol. 8, no. 2, pp. 169–180, 2004.

[59] Y. Wang *et al.*, "Studies on the performance of selective laser melting porous dental implant by finite element model simulation, fatigue testing and in vivo experiments," *Proc. Inst. Mech. Eng. Part H J. Eng. Med.*, vol. 233, no. 2, pp. 170–180, 2019.

[60] N. Lioubavina-Hack, N. P. Lang, and T. Karring, "Significance of primary stability for osseointegration of dental implants," *Clin. Oral Implants Res.*, vol. 17, no. 3, pp. 244–250, 2006.

[61] N. P. Lang, L. Pun, K. Y. Lau, K. Y. Li, and M. C. M. Wong, "A systematic review on survival and success rates of implants placed immediately into fresh extraction sockets after at least 1 year," *Clin. Oral Implants Res.*, vol. 23, no. SUPPL. 5, pp. 39–66, 2012.

[62] W. Pirker and A. Kocher, "Immediate, non-submerged, root-analogue zirconia implants placed

into single-rooted extraction sockets: 2-year follow-up of a clinical study," *Int. J. Oral Maxillofac. Surg.*, vol. 38, no. 11, pp. 1127–1132, Nov. 2009.

[63] T. Grandi, G. Garuti, P. Guazzi, L. Tarabini, and A. Forabosco, "Survival and success rates of immediately and early loaded implants: 12-month results from a multicentric randomized clinical study," *J. Oral Implantol.*, vol. 38, no. 3, pp. 239–249, 2012.

[64] Y. Liu, L. Enggist, A. F. Kuffer, D. Buser, and E. B. Hunziker, "The influence of BMP-2 and its mode of delivery on the osteoconductivity of implant surfaces during the early phase of osseointegration," *Biomaterials*, vol. 28, no. 16, pp. 2677–2686, 2007.

[65] C. Mangano *et al.*, "Prospective clinical evaluation of 201 direct laser metal forming implants: Results from a 1-year multicenter study," *Lasers Med. Sci.*, vol. 27, no. 1, pp. 181–189, 2012.

[66] E. O. Almeida, A. C. F. Júnior, E. A. Bonfante, N. R. F. A. Silva, and P. G. Coelho, "Reliability evaluation of alumina-blasted/acid-etched versus laser-sintered dental implants," *Lasers Med. Sci.*, vol. 28, no. 3, pp. 851–858, 2013.

[67] M. Bächle and R. J. Kohal, "A systematic review of the influence of different titanium surfaces on proliferation, differentiation and protein synthesis of osteoblast-like MG63 cells," *Clin. Oral Implants Res.*, vol. 15, no. 6, pp. 683–692, 2004.

[68] M. Tsukanaka *et al.*, "Bioactive treatment promotes osteoblast differentiation on titanium materials fabricated by selective laser melting technology," *Dent. Mater. J.*, vol. 35, no. 1, pp. 118–125, 2016.

[69] I. A. J. van Hengel *et al.*, "Selective laser melting porous metallic implants with immobilized silver nanoparticles kill and prevent biofilm formation by methicillin-resistant Staphylococcus aureus," *Biomaterials*, vol. 140, pp. 1–15, Sep. 2017.

[70] M. Tierolf, "Antibacterial Surfaces Bearing Silver, Copper and Zinc Nanoparticles on Additively Manufactured Titanium Implants," *Master thesis Delft Univ. Technol.*, pp. 1–52, 2018.

[71] N. E. Putra, "Antibacterial Surfaces Bearing Silver and Zinc Nanoparticles on Additively Manufactured Titanium Implants," *Master thesis Delft Univ. Technol.*, pp. 1–55, 2018.

[72] J. Vaithilingam *et al.*, "Surface chemistry of Ti6Al4V components fabricated using selective laser melting for biomedical applications," *Mater. Sci. Eng. C*, vol. 67, pp. 294–303, 2016.

[73] C. S. Dunleavy, I. O. Golosnoy, J. A. Curran, and T. W. Clyne, "Characterisation of discharge events during plasma electrolytic oxidation," *Surf. Coatings Technol.*, vol. 203, no. 22, pp. 3410–3419, 2009.

[74] F. Muhaffel, G. Cempura, M. Menekse, A. Czyrska-Filemonowicz, N. Karaguler, and H. Cimenoglu, "Characteristics of multi-layer coatings synthesized on Ti6Al4V alloy by micro-arc oxidation in silver nitrate added electrolytes," *Surf. Coatings Technol.*, vol. 307, pp. 308–315, 2016.

[75] T. E. Park, H. C. Choe, and W. A. Brantley, "Bioactivity evaluation of porous TiO2 surface formed on titanium in mixed electrolyte by spark anodization," *Surf. Coatings Technol.*, vol. 235, pp. 706–713, 2013.

[76] Y. T. Sul, "The significance of the surface properties of oxidized titanium to the bone response: Special emphasis on potential biochemical bonding of oxidized titanium implant," *Biomaterials*, vol. 24, no. 22, pp. 3893–3907, 2003.

[77] A. L. Yerokhin, X. Nie, A. Leyland, and A. Matthews, "Characterisation of oxide films produced by plasma electrolytic oxidation of a Ti-6Al-4V alloy," *Surf. Coatings Technol.*, vol. 130, no. 2–

3, pp. 195–206, 2000.

[78] H. Habazaki, M. Uozumi, H. Konno, K. Shimizu, P. Skeldon, and G. E. Thompson, “Crystallization of anodic titania on titanium and its alloys,” *Corros. Sci.*, vol. 45, no. 9, pp. 2063–2073, 2003.

[79] M. Gaintantzopoulou, S. Zinelis, N. Silikas, and G. Eliades, “Micro-Raman spectroscopic analysis of TiO2 phases on the root surfaces of commercial dental implants,” *Dent. Mater.*, vol. 30, no. 8, pp. 861–867, 2014.

[80] H. J. Song, M. K. Kim, G. C. Jung, M. S. Vang, and Y. J. Park, “The effects of spark anodizing treatment of pure titanium metals and titanium alloys on corrosion characteristics,” *Surf. Coatings Technol.*, vol. 201, no. 21 SPEC. ISS., pp. 8738–8745, 2007.

[81] R. Liu *et al.*, “Surface characteristics and cell adhesion: A comparative study of four commercial dental implants,” *J. Prosthodont.*, vol. 22, no. 8, pp. 641–651, 2013.

[82] T. D. P. Busquim, C. N. Elias, J. E. May, S. E. Kuri, and P. A. D. P. Nascente, “Titanium oxide layer on the surface of anodized dental implants,” *Med. Device Mater. V - Proc. Mater. Process. Med. Devices Conf.*, no. February 2016, pp. 60–65, 2010.

[83] Y. T. Sul *et al.*, “Characteristics of the surface oxides on turned and electrochemically oxidized pure titanium implants up to dielectric breakdown: the oxide thickness, micropore configurations, surface roughness, crystal structure and chemical composition,” *Biomaterials*, vol. 23, no. 2, pp. 491–501, 2002.

[84] L. H. Li *et al.*, “Improved biological performance of Ti implants due to surface modification by micro-arc oxidation,” *Biomaterials*, vol. 25, no. 14, pp. 2867–2875, 2004.

[85] J. He *et al.*, “The anatase phase of nanotopography titania plays an important role on osteoblast cell morphology and proliferation,” *J. Mater. Sci. Mater. Med.*, vol. 19, no. 11, pp. 3465–3472, 2008.

[86] B. Del Curto *et al.*, “Decreased bacterial adhesion to surface-treated titanium,” *Int. J. Artif. Organs*, vol. 28, no. 7, pp. 718–730, 2005.

[87] I. Sondi and B. Salopek-Sondi, “Silver nanoparticles as antimicrobial agent: A case study on E. coli as a model for Gram-negative bacteria,” *J. Colloid Interface Sci.*, vol. 275, no. 1, pp. 177–182, 2004.

[88] J. R. Morones *et al.*, “The bactericidal effect of silver nanoparticles,” *Nanotechnology*, vol. 16, no. 10, pp. 2346–2353, 2005.

[89] C. N. Lok *et al.*, “Silver nanoparticles: Partial oxidation and antibacterial activities,” *J. Biol. Inorg. Chem.*, vol. 12, no. 4, pp. 527–534, 2007.

[90] M. Yamanaka, K. Hara, and J. Kudo, “Bactericidal Actions of a Silver Ion Solution on,” *Appl. Environ. Microbiol.*, vol. 71, no. 11, pp. 7589–7593, 2005.

[91] S. Shrivastava, T. Bera, A. Roy, G. Singh, P. Ramachandrarao, and D. Dash, “Characterization of enhanced antibacterial effects of novel silver nanoparticles,” *Nanotechnology*, vol. 18, no. 22, 2007.

[92] S. R. K. Pandian, V. Deepak, K. Kalishwaralal, P. Viswanathan, and G. Sangiliyandi, “Mechanism of bactericidal activity of silver nitrate - A concentration dependent bi-functional molecule,” *Brazilian J. Microbiol.*, vol. 41, no. 3, pp. 805–809, 2010.

[93] K. Chaloupka, Y. Malam, and A. M. Seifalian, “Nanosilver as a new generation of nanoproduct

in biomedical applications," *Trends Biotechnol.*, vol. 28, no. 11, pp. 580–588, 2010.

[94] M. Godoy-Gallardo *et al.*, "Evaluation of bone loss in antibacterial coated dental implants: An experimental study in dogs," *Mater. Sci. Eng. C*, vol. 69, pp. 538–545, 2016.

[95] R. Pokrowiecki *et al.*, "In vitro studies of nanosilver-doped titanium implants for oral and maxillofacial surgery," *Int. J. Nanomedicine*, vol. 12, pp. 4285–4297, 2017.

[96] E. Unosson, D. Rodriguez, K. Welch, and H. Engqvist, "Reactive combinatorial synthesis and characterization of a gradient Ag-Ti oxide thin film with antibacterial properties," *Acta Biomater.*, vol. 11, no. 1, pp. 503–510, 2015.

[97] S. Mei *et al.*, "Antibacterial effects and biocompatibility of titanium surfaces with graded silver incorporation in titania nanotubes," *Biomaterials*, vol. 35, no. 14, pp. 4255–4265, 2014.

[98] P. E. Kolenbrander, R. N. Andersen, D. S. Blehert, P. G. Egland, J. S. Foster, and R. J. Palmer, "Communication among Oral Bacteria," *Microbiol. Mol. Biol. Rev.*, vol. 66, no. 3, pp. 486–505, 2002.

[99] M. C. Sánchez, A. Llama-Palacios, V. Blanc, R. León, D. Herrera, and M. Sanz, "Structure, viability and bacterial kinetics of an in vitro biofilm model using six bacteria from the subgingival microbiota," *J. Periodontal Res.*, vol. 46, no. 2, pp. 252–260, 2011.

[100] M. C. Sánchez *et al.*, "An in vitro biofilm model associated to dental implants: Structural and quantitative analysis of in vitro biofilm formation on different dental implant surfaces," *Dent. Mater.*, vol. 30, no. 10, pp. 1161–1171, 2014.

[101] D. Violant, M. Galofré, J. Nart, and R. Patricio Teles, "In vitro evaluation of a multispecies oral biofilm on different implant surfaces," *Biomed. Mater.*, vol. 9, no. 3, 2014.

7. Appendices

Appendix I

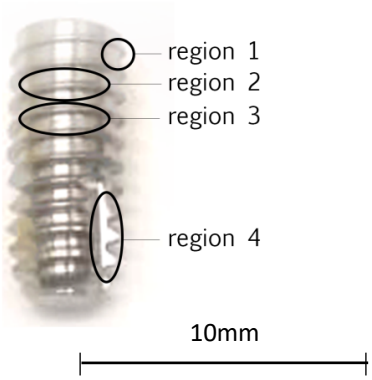

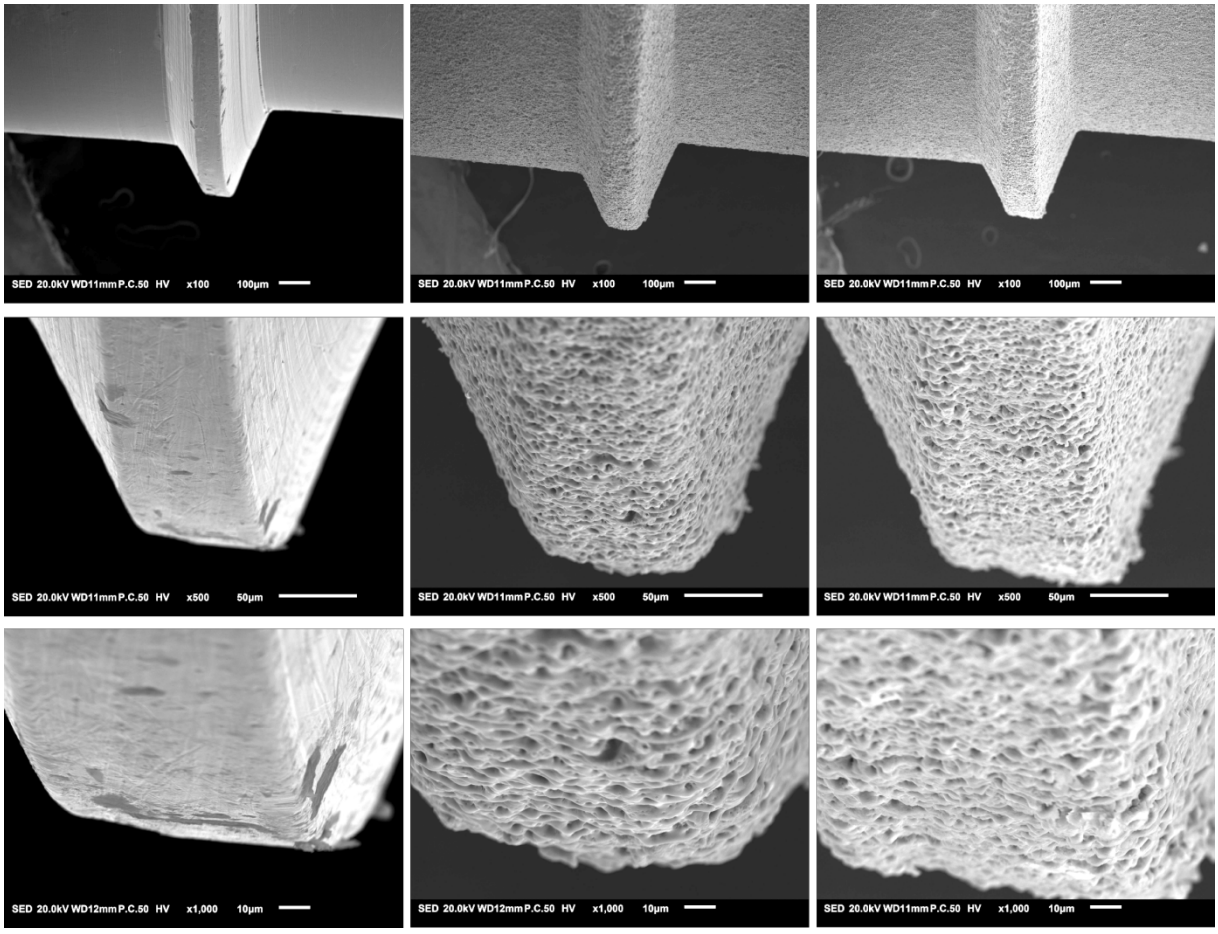

.

(a) (b) (c)

Region 1: End of a thread on the Dyna implant analysed with SEM with a magnification of 100x, 200x and 1000x. (a) non-treated implants. (b) PEO-treated implants. (c) PEO + Ag treated implants.

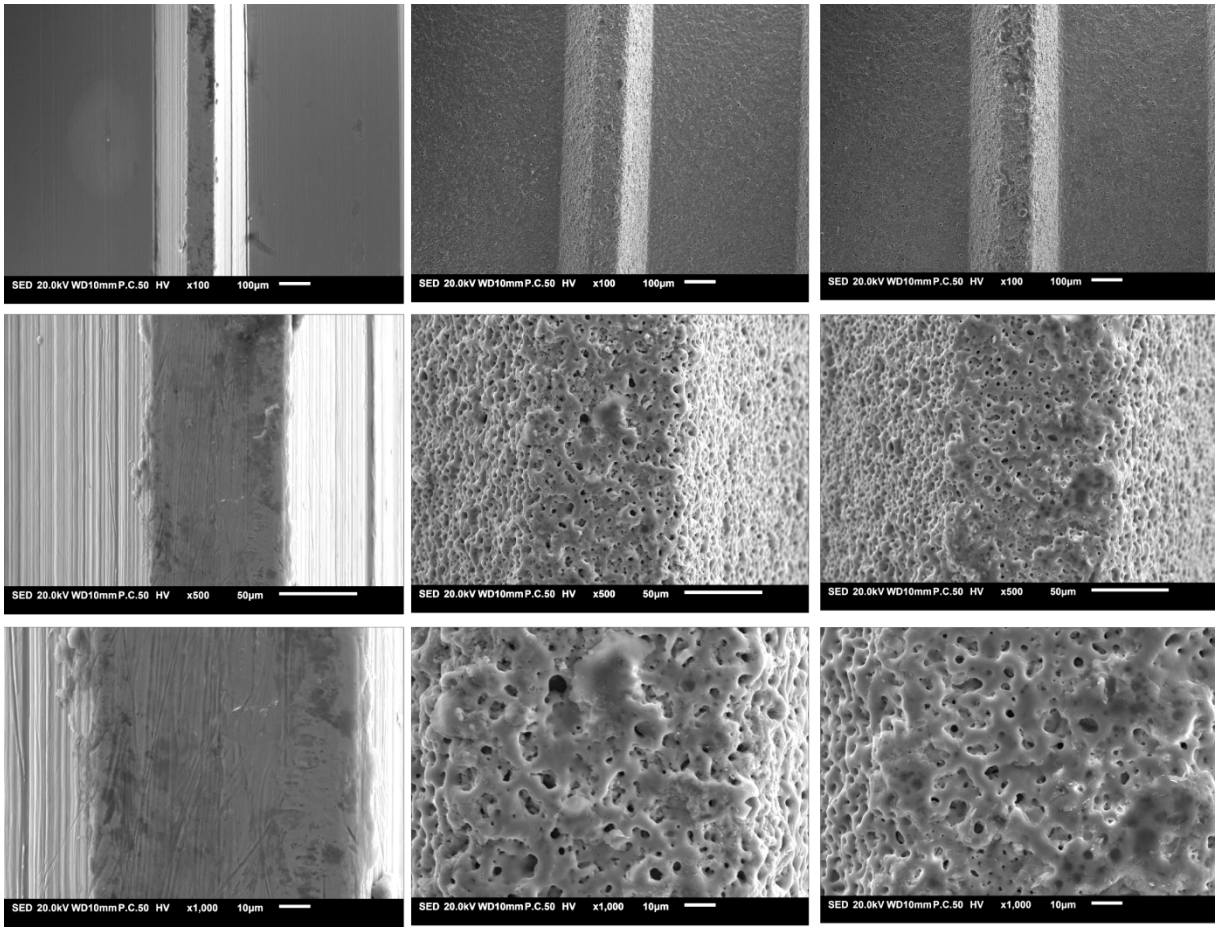

(a) (b) (c)

Region 2: Mi

ddle of a thread on the Dyna implant analysed with SEM with a magnification of 100x, 200x and 1000x. (a) non-treated implants. (b) PEO-treated implants. (c) PEO + Ag treated implants.

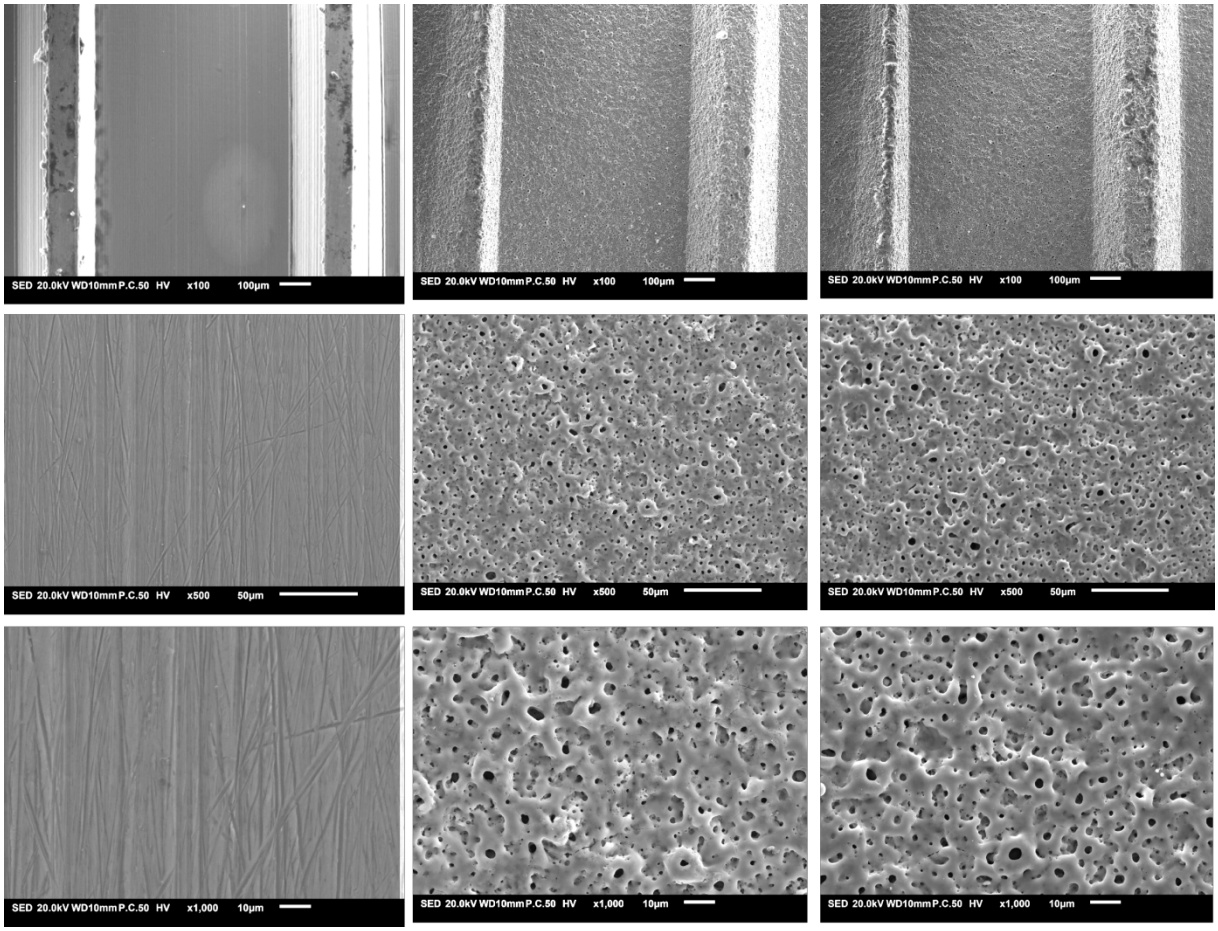

(a) (b) (c)

Region 3: Rounded part of the Dyna implant analysed with SEM with a magnification of 100x, 200x and 1000x. (a) non-treated implants. (b) PEO-treated implants. (c) PEO + Ag treated implants.

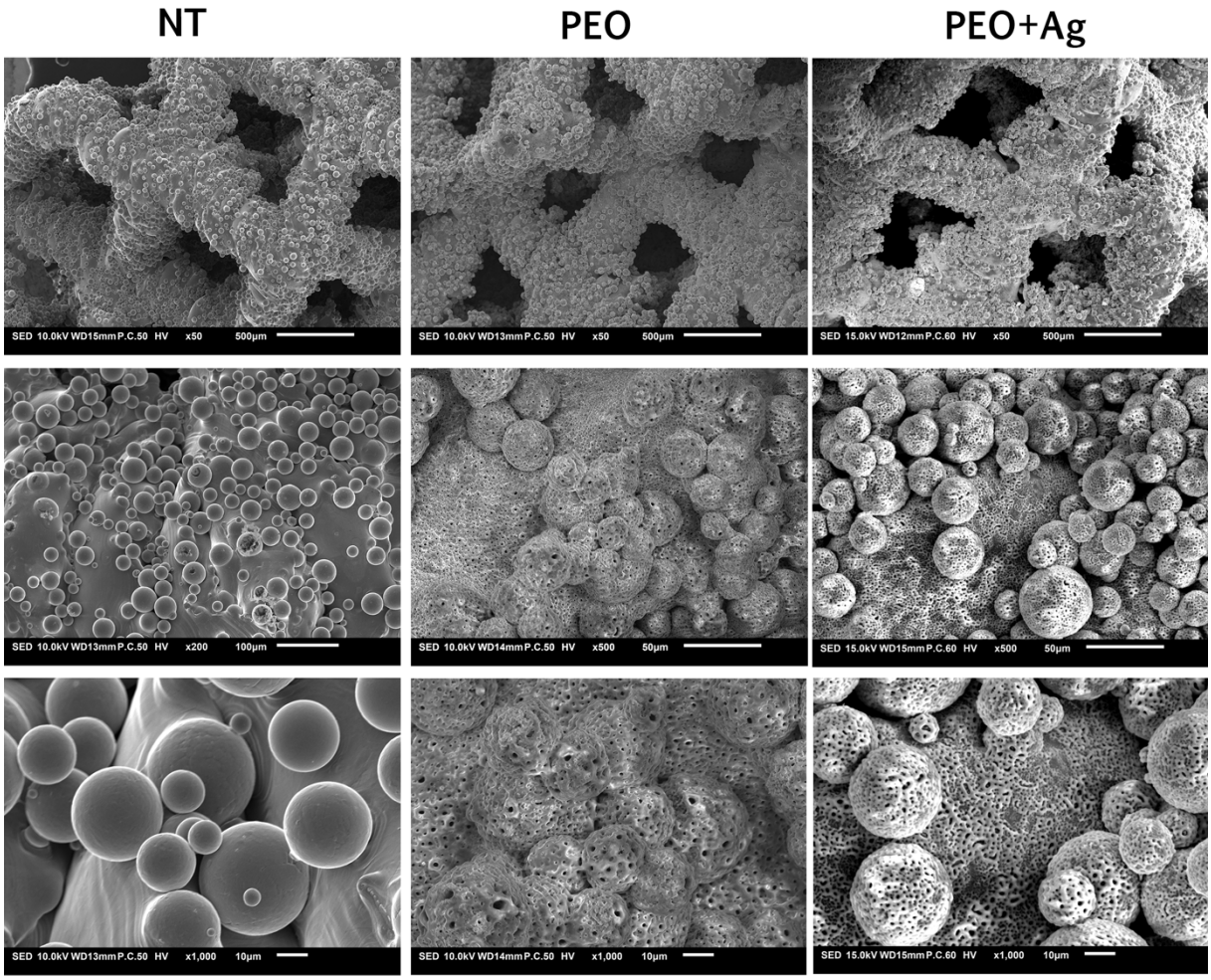

S300 P780 implant analysed with SEM . NT 50x, 200x, 1000x. PEO and PEO+Ag 50x, 500x, 1000x, 2000x.

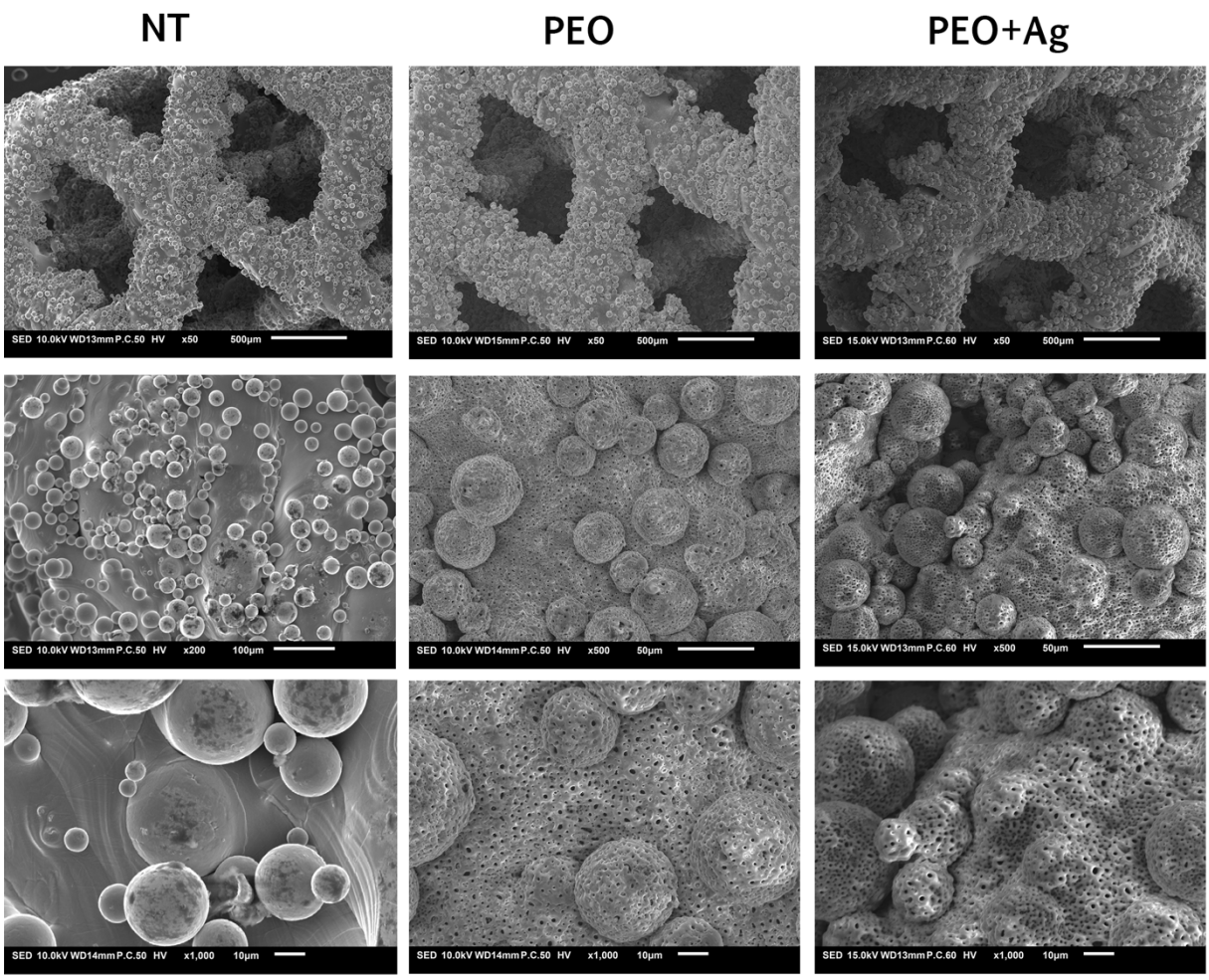

S300 P980 implant analysed with SEM . NT 50x, 200x, 1000x. PEO and PEO+Ag 50x, 500x, 1000x, 2000x.

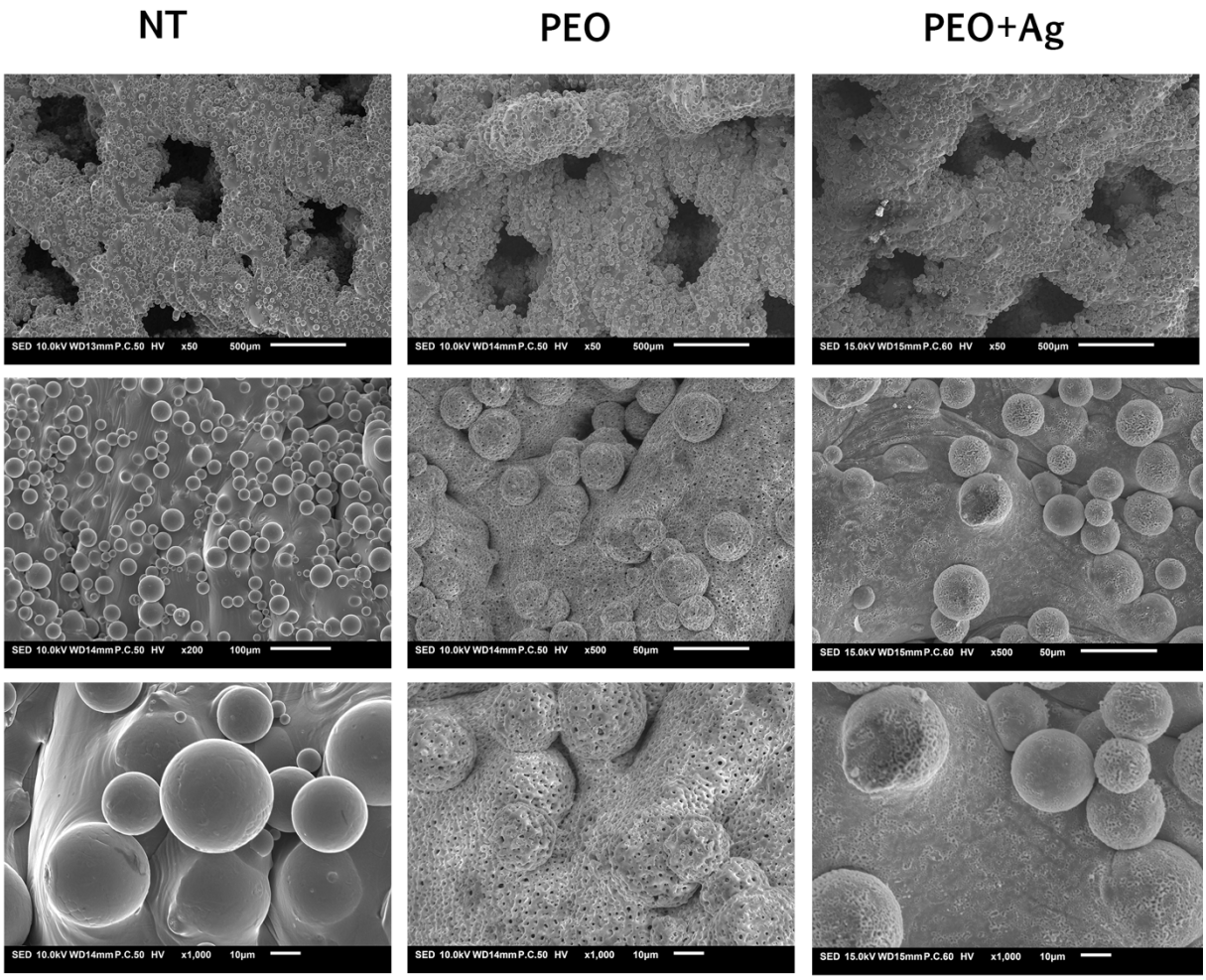

S400 P650 implant analysed with SEM . NT 50x, 200x, 1000x. PEO and PEO+Ag 50x, 500x, 1000x, 2000x.

Appendix II

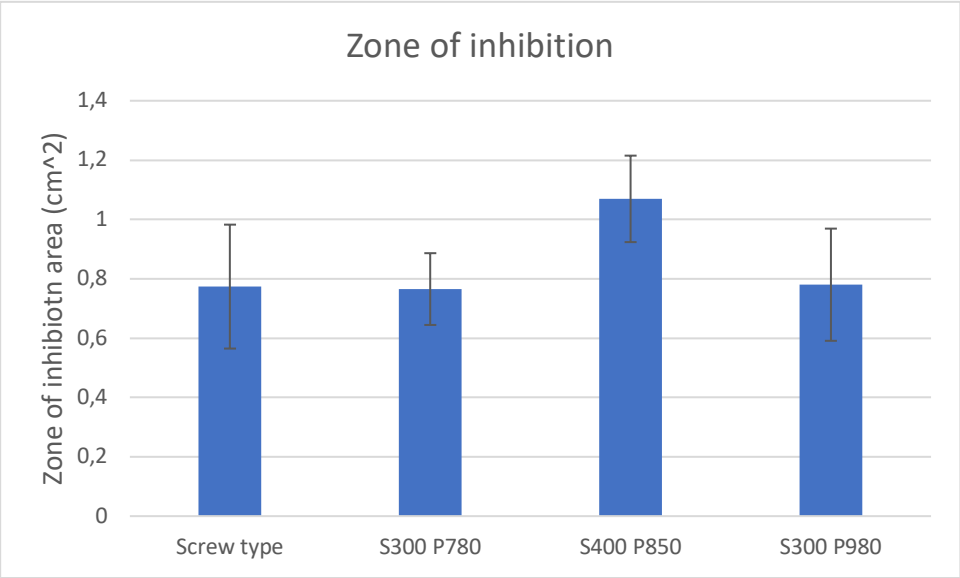

Zone of inhibition of dental implants. This test indicates the zone of inhibition of the dental implants against MRSA. Bars indicated the standard deviation of the results (n=3 for all implants). In this test the porous implants could not lie flat in the agar.

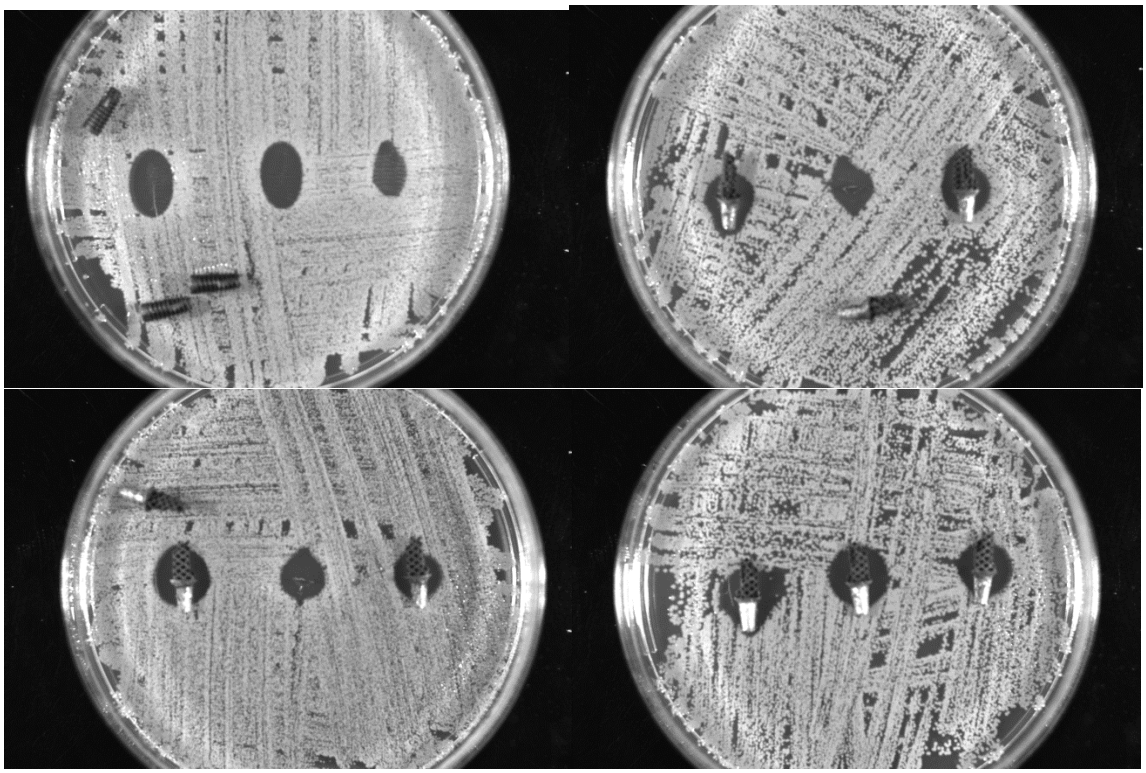

The implants had an extrusion from the abutment, which prevented the implants to be placed flat in the agar assay. This causes small areas in which the implant did not touch the agar, and so the antibacterial properties of the implant were not tested in these areas. The study was done again, by

removing the extrusion of the abutment. This resulted in larger zone of inhibitions for the additive manufactured dental implants.